How to cite: *Angew. Chem. Int. Ed.* **2023**, *62*, e202308891
doi.org/10.1002/anie.202308891

K-ion Batteries

Carbon Electrode Materials for Advanced Potassium-Ion Storage

Wenchao Zhang[+#], Rui Huang[+#], Xu Yan, Chen Tian, Ying Xiao, Zhang Lin, Liming Dai,* Zaiping Guo,* and Liyuan Chai*

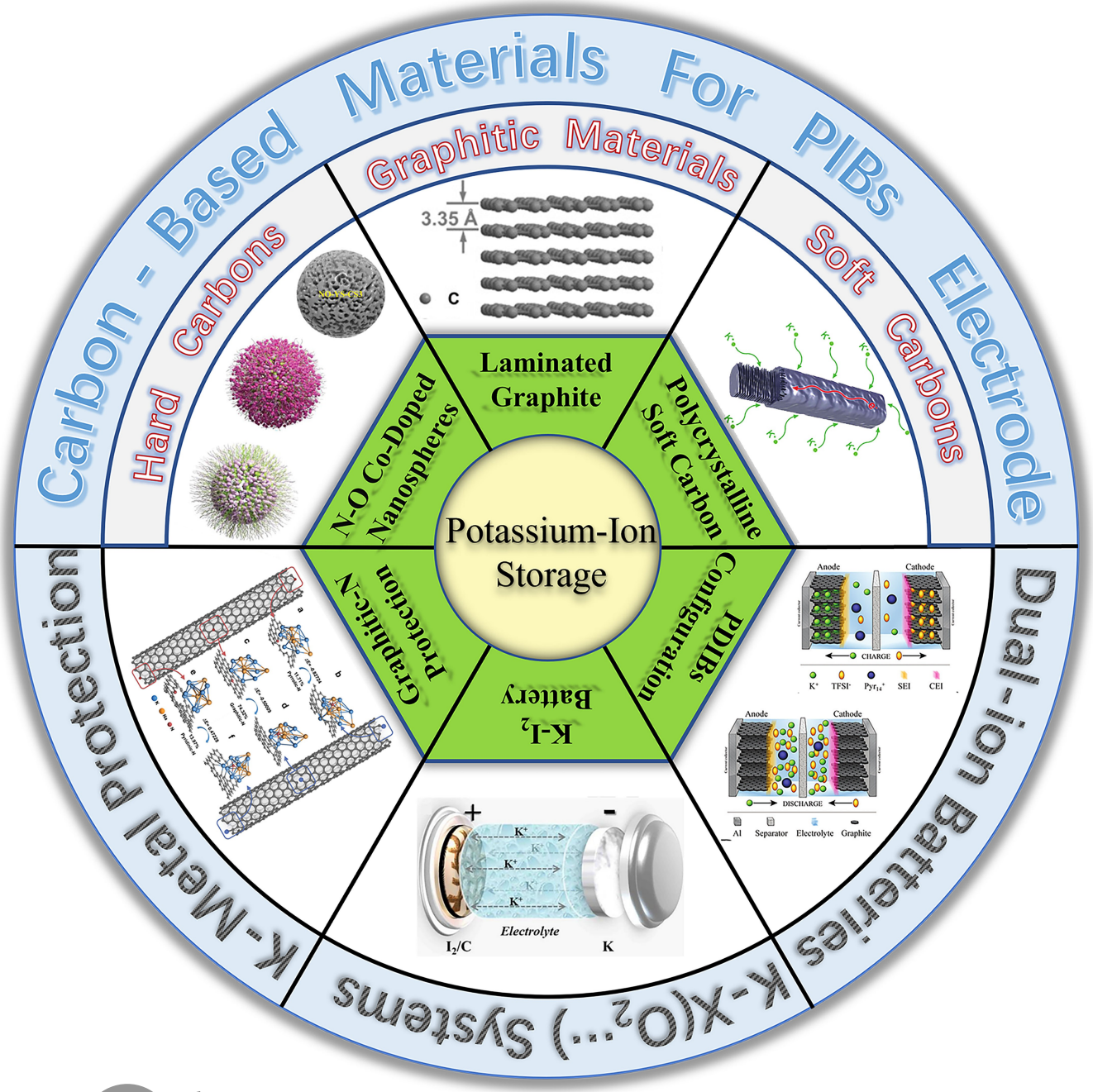

Abstract: Tremendous progress has been made in the field of electrochemical energy storage devices that rely on potassium-ions as charge carriers due to their abundant resources and excellent ion transport properties. Nevertheless, future practical developments not only count on advanced electrode materials with superior electrochemical performance, but also on competitive costs of electrodes for scalable production. In the past few decades, advanced carbon materials have attracted great interest due to their low cost, high selectivity, and structural suitability and have been widely investigated as functional materials for potassium-ion storage. This article provides an up-to-date overview of this rapidly developing field, focusing on recent advanced and mechanistic understanding of carbon-based electrode materials for potassium-ion batteries. In addition, we also discuss recent achievements of dual-ion batteries and conversion-type K–X (X = O_2, CO_2, S, Se, I_2) batteries towards potential practical applications as high-voltage and high-power devices, and summarize carbon-based materials as the host for K-metal protection and possible directions for the development of potassium energy-related devices as well. Based on this, we bridge the gaps between various carbon-based functional materials structure and the related potassium-ion storage performance, especially provide guidance on carbon material design principles for next-generation potassium-ion storage devices.

1. Introduction

Recently, devices relying on potassium ions as charge carriers have attracted wide attention as alternative energy storage systems due to the high abundance of potassium resources (1.5 wt % in the earth's crust) and fast ion transport kinetics of K^+ in electrolyte.[1] Currently, owing to the lower standard hydrogen potential of potassium (−2.93 V vs. E^0) compared to sodium (−2.71 V vs. E^0), potassium ion batteries (PIBs) feature the advantage of high energy density have attracted great interest as an alternative to lithium-ion batteries (LIBs).[2] In addition to PIBs, extended potassium-ion storage systems such as dual-ion batteries and K–X (X = O_2,[3] I_2,[4] S,[5] Se[6]) batteries have been reported and exhibited excellent K^+-storage rate capability. However, the development of potassium-ion storage devices is prominently restricted by the construction of anode. For instance, the metal-free anode is facing several dilemmas: 1) Unstable SEI film, 2) Inevitable structure collapse of anode material upon cycling, 3) Exaggerated pseudocapacitance effects,[7] and 4) Persistent electrolyte consumption and side-reactions.[8] These traps lead to low energy density and the fast capacity decay of PIBs.[9] Moreover, the high reactivity of K-metal anode inevitably generates dendritic metal and unstable solid electrolyte interphase, lead to low Coulombic efficiency and inferior cycling stability.[10]

Nevertheless, numerous strategies to improve the electrochemical performance of PIBs were established on the basis of expensive metal-based materials, various electrolytes, and complex synthesis procedures, which might increase the costs to some extent.[11] Therefore, there were still huge concerns about how to reduce the cost and make potassium storage devices suitable for practical applications. With the great advantages of low cost, carbon materials have been explored as electrode materials for lithium and sodium energy storage devices due to their high abundance, good electrical conductivity, benign tailorable properties, eco-friendliness, and high stability in electrolytes.[12]

Among all the carbon-based materials, carbon tubes (CNTs), graphite, graphene, amorphous carbon, and their derived 3D structures have been considered to be potential candidates, which could be applied in the potassium-ion storage devices.[13] Generally, CNTs possess long and hollow structures with walls formed by atom-thick sheets, and the conjugated all-carbon structure possesses good electrical and mechanical properties, which are promising for PIBs.[14] For 2D structure, graphene with an one-atom-thick planar sheet of sp^2-bonded structure has recently attracted extensive attention for a broad application of potassium-ion storage.[15] The relatively large theoretical specific area (2630 $m^2 g^{-1}$) and good electrical conductivity offered great chances to apply graphene-based materials as PIBs' anode. Recently, hierarchically structured 3D carbon has attracted great interest because they not only offer good electrical conductivity and promising specific surface area, but also can construct stable skeletons to enable fast ion trans-

[*] Prof. W. C. Zhang,[+#] R. Huang,[+#] Prof. X. Yan, Prof. C. Tian, Prof. Z. Lin, Prof. L. Y. Chai
School of Metallurgy and Environment, Central South University
Changsha, 410083 (China)
and
Chinese National Engineering Research Centre for Control & Treatment of Heavy Metal Pollution, Central South University
Changsha, 410083 (China)

Prof. Y. Xiao
Beijing Key Laboratory of Electrochemical Process and Technology for Materials, Beijing University of Chemical Technology
Beijing 100029 (P. R. China)
E-mail: yxiao@buct.edu.cn

Prof. L. M. Dai
Australian Carbon Materials Centre (A-CMC), School of Chemical Engineering, University of New South Wales
Sydney, NSW-2052 (Australia)
E-mail: l.dai@unsw.edu.au

Prof. Z. P. Guo
School of Chemical Engineering and Advanced Materials, The University of Adelaide
Adelaide, SA-5005 (Australia)
E-mail: zaiping.guo@adelaide.edu.au

[+] These authors contributed equally to this work.

[#] co-first authors

portations during electrochemical reactions.[12a,16] Many recent studies have demonstrated that 3D structured carbon-based electrodes could be potentially employed as matrix to protect K-metal anodes and deliver superior electrochemical performance.[17] Besides, the charge transport kinetics and potassiation/depotassiation processes could be further enhanced by heteroatom doping and porous structural design.[18] Due to their abundant potassiophilic surface, low nucleation barrier and stable interaction between carbon-potassium atoms, the K stripping/plating process could be well regulated thus enabling K metal stable. In view of these benefits, there are plenty of new opportunities for the development of advanced carbon-based electrode materials useful for PIBs and new potassium-based energy storage systems.

In this Review, we will first summarize recent developments on carbon-based electrode materials and discuss the mechanism studies that are relevant to PIBs. Different from the few previous review papers focused on electrode materials, this critical Review will focus on recent advances in carbon-based potassium storage devices, including potassium-based dual-ion batteries (PDIBs), conversion-type K–X (X = I_2, O_2, CO_2, S and Se) batteries and K-metal batteries. Finally, possible directions for developing high-performance potassium storage devices will be outlined.

2. Carbon materials for PIBs

Carbon materials generally include graphite, graphene, diamond, and amorphous carbon (soft and hard carbon) based on their different atom arrangements. As the most promising anode material and the one that has undergone successful commercialization in LIBs, graphite has attracted significant interest due to the formation of graphite intercalation compounds (GICs).[19] Graphene is a 2D layer of sp^2 hybrid carbon atoms packed tightly together in a honeycomb lattice with good chemical stability, high electrical conductivity, and excellent reaction kinetics.[20] Based on this, graphene and graphene-based materials have been extensively studied in the use of anode application.[21] To date, it has been demonstrated that graphite and graphene could be intercalated by many chemical species, especially alkali ions such as Li, K, and Rb.[19c] Hard carbons (HCs) are so-called non-graphitizable carbon, and the structure of HCs is constituted by small graphene sheets, amorphous regions with defects, and porosity.[22] Compared with graphite, K ion presents a relatively high diffusion coefficient in HCs, which can not only intercalate into the graphite layers in HCs but also be adsorbed onto the nanovoids and surface defects/functional groups.[23] Unlike the HCs materials, soft carbons (SCs) offer good rate capability and high reversible capacity but undesirable cycling performance. Benefiting from the highly tuneable crystallinity and lattice spacing, SCs also

Ying Xiao is an associate professor at Beijing University of Chemical Technology. She received her PhD degree from Beijing Insinuate of Technology in 2015. From December 2015 to 2019, she worked as a postdoctoral researcher at Hanyang University and BUCT-CWRU International Joint Lab successively. Her current research interests focus on the design and synthesis of key materials for Li/Na-ion batteries and metal-air batteries.

Liming Dai is an Australian Laureate Fellow, Scientia Professor and SHARP Professor at University of New South Wales (UNSW) Sydney. He is also Director of the Australian Carbon Materials Centre and the ARC Centre of Excellence for Carbon Science and Innovation. Before joining UNSW, he was the Kent Hale Smith Professor of polymer science and engineering at Case Western Reserve University. He serves as an Associate Editor of Nano Energy. He is a Fellow of the Royal Society of Chemistry, Fellow of the US National Academy of Inventors, Fellow of the American Institute for Medical and Biological Engineering, member of Academia Europaea, Fellow of the European Academy of Sciences, and Fellow of Australian Academy of Science. Dr. Dai's expertise covers the synthesis, functionalization, and device fabrication of conjugated polymers and carbon nanomaterials for clean energy, environmental remediation, and biomedical applications.

Professor Zaiping Guo is currently an ARC Australian Laureate Fellow at the School of Chemical Engineering, The University of Adelaide. She was elected as a Fellow of the Australian Academy of Science in 2023. She obtained her PhD in Materials Engineering from the University of Wollongong in 2003. Before joining the University of Adelaide, she served as a Distinguished Professor at the University of Wollongong. Her research focuses on the design and utilization of electrode and electrolyte materials for energy storage and conversion, including rechargeable batteries, hydrogen storage, and fuel cells.

could be regulated to satisfy the needs of PIBs in both excellent energy density and stability effectively.[24]

2.1. Graphitic carbon materials

Shifting from LIBs to SIBs is desirable due to the abundant distribution and low cost of Na resources. Unfortunately, graphite cannot be used as anodes for sodium-ion batteries (SIBs) due to the low theoretical capacity for the formation of NaC_{64} compound.[25] The weak interactions between Na^+ and the graphene layers have shown the infeasibility of the Na-GIC battery. Along this line, it might be expected that graphite would not be favourable for the storage of K^+. Interestingly, Ji et al.[26] and Hu et al.[27] reported that K-GIC showed the capability for electrochemical energy storage in PIBs and demonstrated that graphite has ability to form KC_8.[26,28] According to the thermodynamic description, it was proven that C could react with K to form KC_8 compound.[29] Ex situ experimental results also suggested that KC_{36} formed under 0.2–0.3 V. Upon further potassiation, when the potential decreased to 0.01 V, the reaction products went through two-phase (KC_{24} and KC_8) zones and finally yielded pure KC_8 phase. Furthermore, density functional theory (DFT) calculations were carried out to demonstrate the maximum stable stoichiometry of KC_8 compound.[27] The detailed analysis revealed that the formation sequence of K-GIC for PIBs is $KC_{36}\rightarrow KC_{24}\rightarrow KC_8$.

The above discussion shows promising results for developing high-energy-density PIBs due to the low reaction potential required to form K-GIC compounds. Nevertheless, compared with the ~10 % volume expansion of the fully lithiated state with the formation of LiC_6, the relatively large volume expansion of ~61 % during the discharge process makes it kinetically hard to achieve the reversible formation of KC_8. It should be noted that the layered structure of graphite may be disrupted during cycling to block the K ion transportation and thus leads to the poor cycling and rate performance of K-GIC, impeding its practical applications.

In fact, K-GIC has attracted great interest and shown more favourable intercalation than that of Li due to a lower formation enthalpy for KC_8 ($-27.5\ kJ\,mol^{-1}$) compared to LiC_6 ($-16.5\ kJ\,mol^{-1}$).[30] It was reported that the electrochemical reversible capacity of K in graphite as the anode showed a large capacity of 273 $mAh\,g^{-1}$, which will enlighten the exploration of electrode materials for PIBs.[26] In addition to the storage of K^+, graphite has shown a promising higher discharge plateau (0.23 V) than that of lithium inserted in graphite (0.1 V). Therefore, graphite could provide a feasible way to lower the concerns of dendrite growth caused by metal plating/stripping.[27] The large volume expansion (~61 %) could possibly reduce the coulombic efficiency, however, and weak the reaction kinetics, resulting in poor rate capability during cycling (Figure 1a).[26] On this basis, a new type of polynanocrystalline graphite (PG) was designed by using porous carbon as an epitaxial template.[31] This structure retained highly crystallized characteristic properties in short-range dimensions, but otherwise resembled long-range disordered carbon. The as-prepared PG electrode exhibited stable cycling, with over 50 % capacity retention after 240 cycles. Modified Hummers' method was employed to transform the confined graphite into onion-like carbon (GOC) (Figure 1b). Benefiting from the stable helical structure with plenty of wavy wrinkles, expanded graphitic onion-like carbon (EGOC) anodes exhibited high reversible capacity (404 $mAh\,g^{-1}$ at

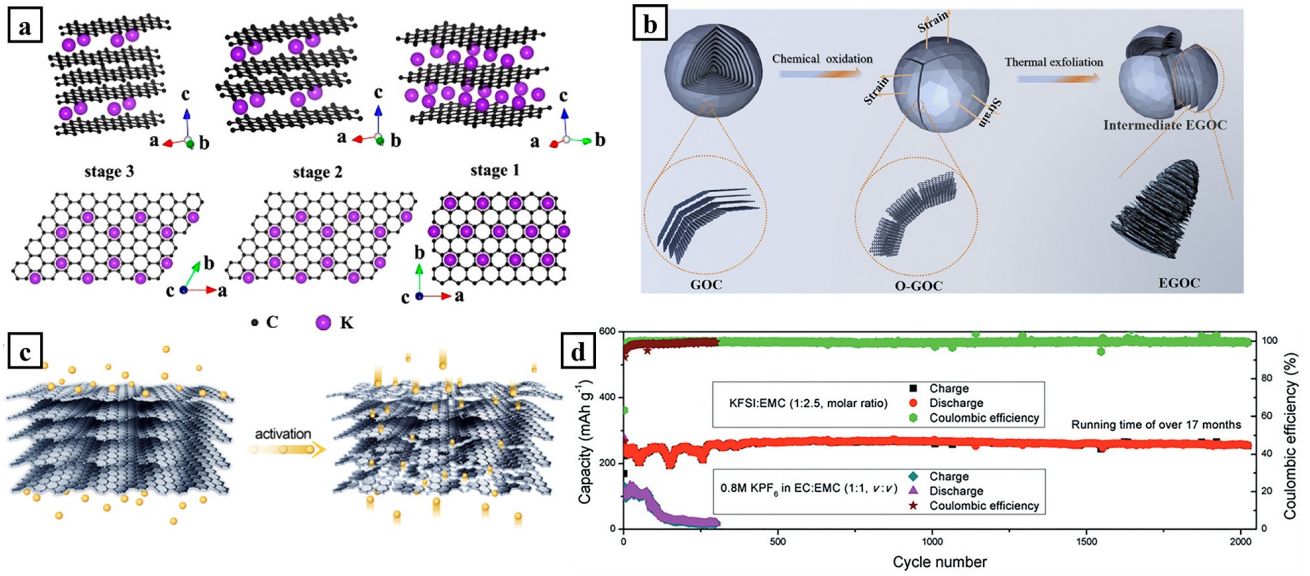

Figure 1. a) Structure diagrams of different K-GICs.[26] Reprinted from Jian et al., with permission. Copyright © 2015, American Chemical Society; b) Structural transition from GOC to EGOC.[32] Reprinted from Meng et al., with permission. Copyright © 2022, Royal Society of Chemistry; c) Schematic illustration of the evolution of the surface on the graphite.[2c] Reprinted from Tai et al., with permission. Copyright © 2017, Elsevier Ltd.; d) Cycle performance of graphite with two different electrolytes at approximately C/3 (1 C = 279 $mA\,g^{-1}$).[34] Reprinted from Lu et al., with permission. Copyright © 2019, John Wiley and Sons.

0.2C), outstanding rate capability (218 $mAh\,g^{-1}$ at 5C) and superior cyclability (275 $mAh\,g^{-1}$ after 1000 cycles at 2C).[32]

In order to take the volume variations into account and increase the Coulombic efficiency during cycling, it is worth paying attention to the effects of the electrolyte and the binder. In view of this, Wang et al. reported that KS4 graphite in KPF_6: ethylene carbonate- propylene carbonate (EC:PC) electrolyte showed superior cycling performance with a capacity of 220 $mAh\,g^{-1}$ after 200 cycles and exhibited a higher initial Coulombic efficiency than in diethyl carbonate (DEC) or dimethyl carbonate (DMC) electrolyte.[33] This is probably due to the severe decomposition and reduction of DEC and DMC under relatively low voltage, which indicated that more cycles were needed to form a stable solid-electrolyte interphase (SEI) layer in DEC-based electrolyte. Furthermore, it could be speculated that more electrolytes would be continuously consumed in dimethoxyethane (DME) or DMC electrolyte compared with that in PC electrolyte. Besides, the binder is also the key to improving cyclability due to its important adhesive function, thus enhancing electrode integrity upon cycling. As a result, by using sodium carboxymethyl cellulose (Na-CMC) binder, the electrode showed higher Coulombic efficiency than that with conventional polyvinylidene difluoride (PVDF) in graphite. It is possible that Na-CMC could provide a uniform coating layer to reduce the consumption of electrolytes in forming the SEI layer.

The obstacles to ionic transportation for K^+ insertion into graphite is mainly caused by the narrow interlayer spaces (0.342 nm) and the long diffusion pathways. To address this concern and facilitate K^+ transportation, expanded graphite materials with large interlayer spacing were studied as anodes for PIBs. Figure 1c shows that the activated carbon with an expanded interlayer spacing of 0.358 nm, prepared from the commercial graphite precursor, exhibited around 7 times faster K^+ diffusion with a diffusion coefficient larger than that of commercial graphite.[2c] A recent report[35] also revealed that an expanded graphite electrode with an interlayer spacing of 0.387 nm could deliver a high reversible capacity of 263 $mAh\,g^{-1}$ at 10 $mA\,g^{-1}$ and maintain 174 $mAh\,g^{-1}$ at 200 $mA\,g^{-1}$. Recently, Lu et al. reported that graphite anode could work well by using a concentrated electrolyte to form a robust inorganic-rich passivation layer. The results demonstrated that graphite anode could work over 2000 cycles with barely capacity decay (Figure 1d). It brought our attention to the observation that graphite could maintain its relatively flat discharge/charge plateau after such long cycles.[34]

Generally, the layered structure of graphite revealed an appropriate application prospect for anodes in PIBs, and the expanded graphite materials with large interlayer spacing process superior potassium-ion storage ability. In addition, the employment of different types of electrolytes and binders also affect the properties of layered graphite, the persistent consumption of electrolyte by intrusion into the layered structure will lead to the structural collapse of the graphite. Thus, a reasonable design, such as expanding interlayer spacing, constructing efficient electrolyte/ions pathways, and introducing heteroatoms/intrinsic defects, could form a stable SEI layer in the electrode and electrolyte interface, which is the key to ensure the application of graphite-based material for anodes in PIBs.

The volume expansion of K-GIC is still the main obstacle that limits the cycle life of PIBs. Therefore, it is desirable to design a stable structure that has enough space to accommodate volume variations during cycling. Recently, metal–organic frameworks (MOFs)-derived carbon-based nanomaterials have received significant attention in K^+-storage areas. The metal component could act as a good catalyst to regulate the various structures and morphologies under controllable experimental conditions, and the thus-formed carbon framework can efficiently allocate the stress induced by the potassiation processes. Xu et al. reported a facile way to prepare N-doped carbon nanotubes that relied on zeolitic imidazolate frameworks (ZIFs) as precursor.[36] This structure not only retained mainly graphitic characteristics, but also increased the surface area and shortened the diffusion distance of K^+ to improve the reaction kinetics (Figure 2a). Consequently, the majority capacity contribution corresponding to the potassiated voltage plateau could still be maintained below 0.5 V, demonstrating that the K^+ storage did not depend on the capacitive storage mechanism. Recently, ZIF-8 was used as a self-sacrifice template to design carbon-coated Fe_3C electrode materials with nitrogen doping (Fe_3C@MOF–C/N), which possessed different pore-size distribution, high specific surface area, and graphitization degree (Figure 2b). Owing to the graphite carbon framework with a well-maintained integral structure, the K^+ diffusion pathway was significant shortened due to the large specific surface area and the Fe_3C nanoparticles wrapped with graphite carbon could further prevent the material's pulverization.[37]

In addition, hollow structures have also attracted considerable attention because they offer enough room to buffer the volume expansions and short diffusion channels to facilitate ionic transportation. The preparation of hollow carbon structures generally needs complex routes, however, and suffers from a low yield. Hollow carbon nanospheres (HCNs) were synthesized through a template method (Figure 2c),[38] which presented uniform shells and cavities for K^+ storage. The primary results show a high reversible capacity of 298 $mAh\,g^{-1}$ at 28 $mA\,g^{-1}$ and high-rate capability of 212 $mAh\,g^{-1}$ at 558 $mA\,g^{-1}$. Recently, Wu and co-worker reported nitrogen phosphorous co-doped hollow carbon nanofibers (PNCNFs) derived from high-energy metal–organic frameworks (MOFs) (Figure 2d). The as-prepared anodes show ultra-high N/P co-doping characteristics with some graphentic nanodomains, which resulted in a high reversible capacity (466.2 $mAh\,g^{-1}$) and superior rate capability (244.4 $mAh\,g^{-1}$ at 8 $A\,g^{-1}$).[39]

Although the carbon shell could form a uniform layer and uniform morphology, this layer could not retain highly graphitic characteristics to lower the discharge plateau, thus decreasing the energy density. Our group recently proposed a cage-like graphitic structured carbon that not only effectively reduced the anisotropy to avoid interlayer slipping, thus ensuring structural integrity, but also offered hollow structures to accommodate strain relaxation upon

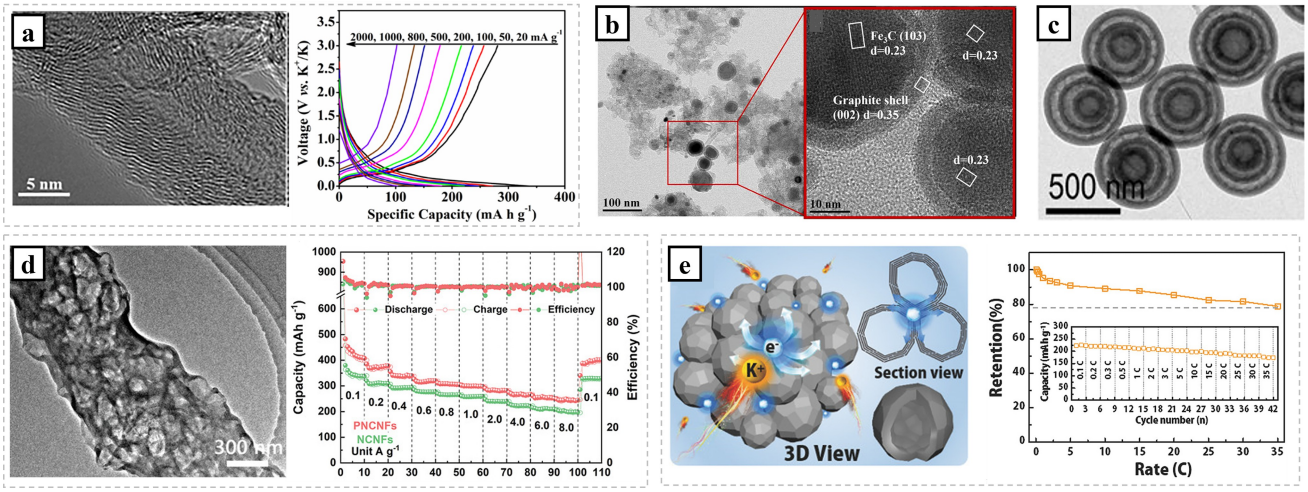

Figure 2. a) TEM image and charge/discharge profiles of the nitrogen-doped carbon nanotubes (NCNTs).[36] Reprinted from Xu et al., with permission. Copyright © 2017, John Wiley and Sons; b) TEM and HRTEM images of Fe_3C@MOF–C/N-1.[37] Reprinted from Xie et al., with permission. Copyright © 2022, Elsevier Ltd.; c) TEM image of three-shelled hollow nanospheres.[38] Reprinted from Bin et al., with permission. Copyright © 2017, American Chemical Society; d) TEM image and rate capability of PNCNFs.[39] Reprinted from Wu et al., with permission. Copyright © 2021, John Wiley and Sons; e) Schematic structural illustration and rate capability of carbon nanocage (CNC).[40] Reprinted from Song et al., with permission. Copyright © 2018, John Wiley and Sons.

cycling (Figure 2e).[40] In addition, this carbon nanocage (CNC) has an even hollow structure with a thin shell thickness of around 5 nm, which could further reduce the ionic diffusion length to improve the chemical diffusivity. The as-prepared CNC electrode could deliver 175 mAh g^{-1} at around 10 A g^{-1}.[34] To the best of our knowledge, this is the best electrochemical performance for highly graphitic electrode materials.

Graphene materials is composed of a single layer or few layers of sp^2 hybridized carbon atoms, owning characteristic chemical and physical properties, such as high electrical conductivity, excellent mechanical strength, large surface area, and large carrier mobility.[21,41] Different from graphite with several graphene layers, two-dimensional graphene nanomaterial is available to enlarge the potassium storage site by hosting K both on and under the aromatic ring as well as additional defects.[18,42] Since the first use of reduced graphene oxide as anode for potassium ion batteries by Luo and co-workers, extensive researches have been reported exploring the potassium storage properties of graphene, graphene oxide, reduced graphene oxide.[43] On the one hand, K possesses a lower migration activation energy in the surface of graphene materials (0.10 eV, 0.14 eV, 0.29 eV for K, Na and Li, respectively), exhibiting stronger ion diffusion kinetics.[44] On the other hand, graphene-based materials can introduce new structures with more defects, edges, grain boundaries, and doped atoms to enhance their potassium storage capacity,[45] and graphene themselves can also be used as functional additives to optimize the properties of other anode materials.[21] Due to the large pseudocapacitance and structural instability of graphene-based materials, the capacity and cycling performance is still inferior to that of counterpart in PIBs, but its unique two-dimensional structure and physicochemical properties are expected to achieve potassium storage under extreme conditions.

As mentioned above, effective strategies have been proposed for graphite structures to facilitate potassium ion diffusion and alleviate lattice expansion. By employing precursors such as MOF, shell and hollow carbon have been used as a template to regulate and control the structure of graphited carbon framework composites. In addition, the heteroatom(s) doping could further improve the power/energy outputs with long-life cycling.

The key to developing highly graphitic electrode materials for practical application in PIBs depends on addressing the poor kinetics of K-GIC reactions. We envisioned that there might be a few principles to follow: a) increase the surface area to enable the electrolyte to come into complete contact with the electrode; b) design nanosized graphitic structures to shorten the diffusion distance, thus improving reaction kinetics; c) build suitable architectures to allow more K^+ ion storage and keep the structure stable during cycling; and d) retain enough crystallinity in the graphitic carbon to keep the discharge voltage potential below a certain level to ensure high-energy-density for PIBs.

2.2. Hard Carbon and Soft Carbon materials

Hard carbon is so-called non-graphitizable carbon and is considered as the most promising anode material for SIBs because graphite is thermodynamically limited in its reactions with sodium.[46] Generally, hard carbon could deliver higher specific capacity compared with graphite electrode materials because the random alignment of graphene layers in a small-sized domain offers significant porosity for storing ions.

Ji et al. first prepared hard carbon spheres (HCS) with diameters of around 5~10 μm via a hydrothermal method (Figure 3a).[47] The obtained HCS electrode exhibited a

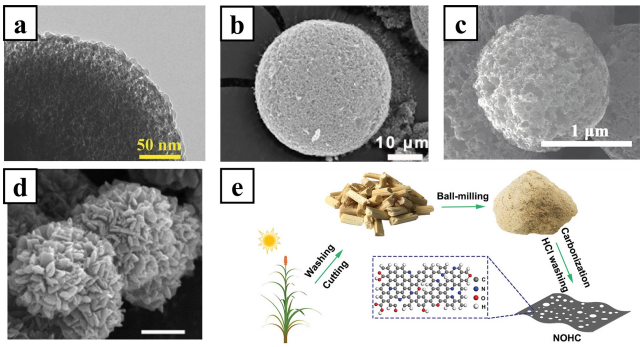

Figure 3. a) Scanning electron microscope (SEM) image of as-prepared HCS.[47] Reprinted from Ji et al., with permission. Copyright © 2015, John Wiley and Sons; b) SEM image of NCS.[49] Reprinted from Chen et al., with permission. Copyright © 2017, Elsevier Ltd.; c) SEM image of porous carbon microspheres (PCMs).[51] Reprinted from Yang et al., with permission. Copyright © 2018, John Wiley and Sons; d) SEM image of the carbonized product of the NH2-MIL-101(Al) precursor.[53] Reprinted from Xiong et al., with permission. Copyright © 2017, John Wiley and Sons; e) Schematic illustration of the preparation of N/O-dual doped hard carbon.[54] Reprinted from Jiang et al., with permission. Copyright © 2020, John Wiley and Sons.

potassiation potential (0.2 and 0.33 V) that was higher than its sodiation potential (lower than 0.1 V), which reduces the risks of dendrite formation, especially at high current rates. It is interesting that HCS electrodes showed higher rate retention ratios for PIBs (52 %) than for SIBs (23 %) at 5C compared to C/10. This excellent rate capability of HCS electrode for PIBs could be possibly attributed to their greater proportion of nanovoids than in the structure of graphite and the higher diffusion coefficient for K^+ diffusivity in hard carbon. Inspired by this pioneering work, Zhong et al. incorporated graphene oxide in renewable lignin precursors to obtain the crystalline lattice hard carbon.[48] The modified hard carbon (i.e., QLGC) anodes show graphitized nanodomains in the carbon matrix with an expanded interlayer spacing (0.42 nm) in the amorphous regions. Xie and co-workers prepared N-doped hard carbon microspheres via directly pyrolyzing cross-linked hierarchically porous chitin microspheres[49] (Figure 3b). Although the majority of the capacity contribution was over 0.5 V, the obtained ultrahigh rate capability of 105 mAh g^{-1} at around 20 A g^{-1} could encourage research work on the exploration of hard carbon microsphere materials. Heteroatom-doping is an efficient way to regulate the local electronic structure and introduce defects/vacancies.[50] In this regard, Yang and Guo et al. prepared porous hard carbon microspheres (Figure 3c).[51] The introduction of S- and O- dual doping to achieve functional bonds with carbon, could further create some vacancies and active sites to increase the adsorption of K ions, which would increase the specific capacity and yield good rate capability (over 150 mA g^{-1} at 1 A g^{-1}). In addition, nitrogen and oxygen co-doped yolk-shell carbon sphere (NO-YS-CS) was prepared as anodes for PIBs, which show ultralong cycling life over 2500 cycles with the retention of 85.8 % at 500 mA g^{-1} and superior rate performance (183.3 mAh g^{-1} at 1.0 A g^{-1}).[52]

Ju and Xiong et al. prepared nitrogen/oxygen dual-doped hard carbon, which exhibited uniform flower-like microspheres with sizes of around 2 micrometres (Figure 3d).[53] N-doped carbon, as an alternative, could regulate the electronic structure to improve the electronic conductivity of the hard carbon, thus further enhancing the cycling performance. A very recent report shows a low-cost method to prepare N/O-dual doped hard carbon relying on biomass resources (Figure 3e). The introduction of heteroatom(s) doping could generate abundant defects, which significantly increase electrochemical active sites.[54]

Hard carbon electrode materials usually suffer from low coulombic efficiency due to the limited reversible capacity since the capacity contribution is mostly consumed by the formation of the SEI layer. The next stage of developing hard carbon anode materials ought to focus on how to design suitable protective layers to avoid the consumption of electrolyte during the formation of the SEI layer.

The early research on soft carbon electrodes was carried out by Ji et al. in 2015, in which soft carbon was considered as a good resource for PIBs due to the less crystalline structure and lower density than graphite.[26] The classic pyrolysed soft carbon from 3, 4, 9, 10-perylene-tetracarboxylicacid-dianhydride (PTCDA) was tested as anode for PIBs, and it delivered better cycling performance and rate capability than t graphite. By integrating the advantages of the long-term cyclability of hard carbon and the high-rate capability of soft carbon, their group reported that the combination of hard carbon spheres, and soft carbon (HCS-SC) display a broad XRD peak with a large average *d*-spacing of 0.37 nm (Figure 4a) and show spherical particles sized from 5–10 μm with micrometer-sized soft carbon rods.[55] The as-prepared HCS-SC electrode delivered a high reversible capacity of over 200 mAh g^{-1} at 280 mA g^{-1} with stable cycling after 200 cycles, and it retained around 100 mAh g^{-1} at 2800 mA g^{-1} (Figure 4b). It should be noted that this work highlights the concept that non-graphitic structure with a high level of disorder along the *c*-axis is critical to avoid capacity fading for carbon-based anodes. To further develop advanced soft carbon anodes, Mai et al. designed polycrystalline soft carbon semi-hollow microrods, which consisted of cavities and nanosheets as anode for PIBs.[56] With the benefits of a hollow structure for accommodating volume variations, short diffusion paths for improving ionic kinetics, and a large electrolyte/electrode contact area (Figure 4c), the electrode delivered a high reversible capacity of 170 mAh g^{-1} at 500 mA g^{-1} with capacity retention of over 80 % after 500 cycles. In addition to half-cell research, they have tested $K_{0.6}CoO_2$//soft carbon in full-cell configurations,[56] which exhibited 86.7 % of the initial coulombic efficiency and 84 % capacity retention after 50 cycles at 20 mA g^{-1}.

Unlike hard carbon materials, soft carbon offers good rate capability and high reversible capacity but undesirable cycling performance. Besides, the large capacity contribution from the high voltage region (>1 V) will diminish its potential as potential high-energy-density anode materials.[24] Therefore, it is worthwhile to design dedicated nanostructures for soft carbon to increase its electrical

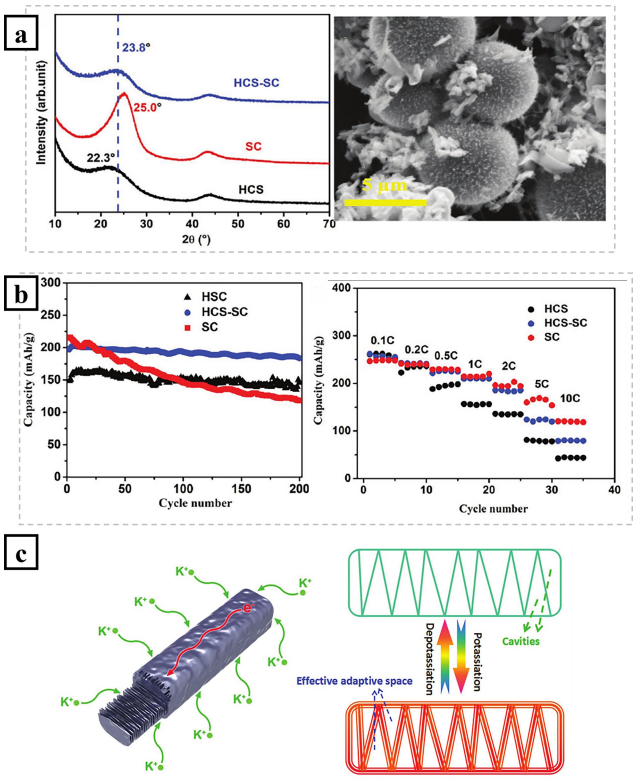

Figure 4. a) XRD patterns and SEM image of the as-prepared composites.[55] Reprinted from Ji et al., with permission. Copyright © 2017, John Wiley and Sons; b) Cycling and rate performance of hard/soft carbon electrodes.[55] Reprinted from Ji et al., with permission. Copyright © 2017, John Wiley and Sons; c) Schematic illustration of a polycrystalline soft carbon semi-hollow microrod.[56] Reprinted from Wang et al., with permission. Copyright © 2017, Royal Society of Chemistry.

conductivity, but also give it enough space to accommodate potassium ions during cycling. For example, hollow structures could buffer the volume expansion during potassiation to extend the lifespan of the cell. Moreover, the development of hard-soft carbon composites is expected to utilize the advantages of the two kinds of carbon and synergistic mutual effects to improve the electrochemical performance of PIBs.

The superior cycling stability and rate capability of hard/soft carbon are due to the large pseudocapacitance contribution upon cycling. Basically, the majority of capacity contributions are driven by surface reactions that do not need diffusion processes, which facilitate the ions/electrons transportations, thus benefiting to improve electrochemical performance. In 1971, the first evidence of pseudocapacitance involving faradaic charge-transfer reactions was discovered in RuO_2 electrode.[57] It was mainly found that the faradaic charge-transfer reaction represented ion storage from the solvents. In addition to this, the shape of the cyclic voltammogram (CV) curve was mostly rectangular, which was attributed to capacitor-type behaviour. In terms of the electrochemical capacitive features, pseudocapacitive mechanisms can be classified into three different types, including redox, intercalation, and underpotential deposition psedocapacitance.[58] The classic intercalation reaction mechanism shares similar processes with co-insertion and K-GIC for PIBs. In contrast, redox pseudocapacitance can store ions on the surface of the electrode material with a concomitant faradaic charge-transfer reaction. All these reaction mechanisms depend on the physical and surface properties of the materials.

In particular, for energy storage behaviour, the pseudocapacitance could be decided by the voltage sweep in CV, with constant or alternating current. In terms of CV tests, the relationship could be written by the following equation:[59]

$$i(V) = k_1 v^{1/2} + k_2 v$$

Where v represents the sweep rate, k_1 and k_2 are parameters that should be taken from the current relationships. In this equation, the current response that varies with v is responsible for the surface-driven behaviour, and $v^{1/2}$ reflects the diffusion-controlled process. According to this method, Xie et al. calculated the surface-driven and diffusion-controlled contributions to the total capacitive charge.[49] The high value of 83 % for the cell at a scanning rate of 2 $mV\,s^{-1}$ demonstrated that the storage was mainly controlled by the capacitive surface-driven process. In addition, the surface-driven storage increases with increasing sweep rate, and the capacitive charge contribution is higher for a K cell than a Na cell.

In the previous sections, we presented the early research on soft carbon and also proposed that nanostructures with enough voids/spaces could benefit the electrochemical performance of soft carbon electrodes. Here, we offer a deeper understanding of the development of carbon fibers and porous carbon electrode materials. Besides, we emphasize that the redox pseudocapacitance reaction mechanism could occur when the ions are adsorbed onto the surface of the electrode materials. The transportation processes mainly depend on the kinetic behaviour, but a few are limited by solid-state diffusion processes. In terms of this reaction mechanism, the majority capacity contribution stems from the surface storage, which maintains the structure of the carbon due to the reduced K-GIC intercalation reactions, thus enabling high-rate cyclability. In this regard, carbon fibers were introduced by the electrospinning technique, which exhibited cross-linked morphology with relatively uniform diameters of 200–300 nm (Figure 5a)[60] and 30–40 nm (Figure 5b),[61] respectively. Furthermore, nitrogen species were introduced for doping onto carbon to increase the density of active sites and produce defects for ion storage. It is interesting to correlate the electrochemical performance with the N dopant content. Based on their X-ray photoelectron spectroscopy (XPS) analyses, a higher N doping level could increase the contribution from pseudocapacitance thus enhancing the reversible capacity (146 $mAh\,g^{-1}$ at 2 $A\,g^{-1}$ after 4000 cycles) and rate capability (101 $mAh\,g^{-1}$ at 20 $A\,g^{-1}$). Motivated by the large surface

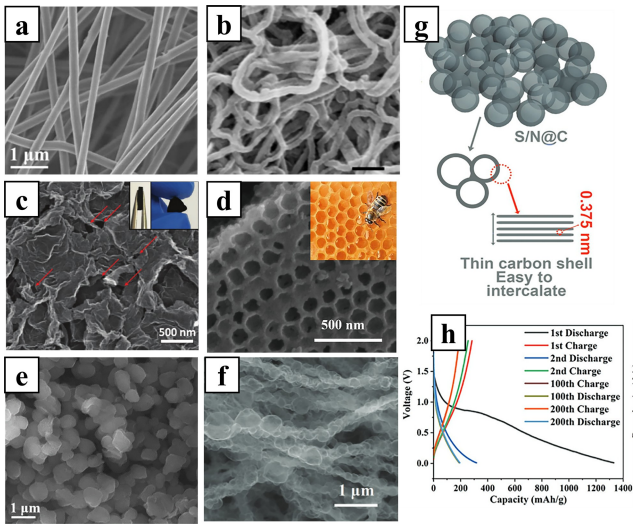

Figure 5. Microscopic characterizations of N-doped carbon fibers with relatively uniform diameters of a) 200–300 nm.[60] Reprinted from Zhao et al., with permission. Copyright © 2017, Royal Society of Chemistry and b) 30–40 nm.[61] Reprinted from Xu et al., with permission. Copyright © 2018, Springer Nature; c) SEM image of the as-synthesized porous carbon monolith (PNCM) (insets are the optical images of the monolithic structure).[66] Reprinted from Qiao et al., with permission. Copyright © 2017, Elsevier Ltd.; d) SEM image with honeycomb shown in the inset for comparison.[63] Reprinted from He et al., with permission. Copyright © 2019, Elsevier Ltd.; e) SEM image of mesoporous carbon.[64] Reprinted from Guo et al., with permission. Copyright © 2017, John Wiley and Sons; f) SEM image of the necklace-like hollow carbon (NHC) sample.[67] Reprinted from Yang et al., with permission. Copyright © 2019, Royal Society of Chemistry; g) Schematic representation of hierarchically porous thin carbon shell of S/N@C.[68] Reprinted from Zhao et al., with permission. Copyright © 2018, John Wiley and Sons; h) Discharge/charge curves for S/N@C electrode materials at 100 mA g^{-1} for PIBs.[68] Reprinted from Mahmood et al., with permission. Copyright © 2018, John Wiley and Sons.

area of porous carbon, Chen, Yan, et al. reported N-doped porous carbon monolith with surface area of around 443 $m^2 g^{-1}$ (Figure 5c).[49] The as-prepared electrode could deliver a stable reversible capacity of over 150 mAh g^{-1} at 1000 mA g^{-1} after 3000 cycles and a high-rate capability of 178 mAh g^{-1} at 5000 mA g^{-1}. In addition, they adopted PTCDA as a cathode to assemble full cells, which delivered over 100 mAh g^{-1} at 500 mA g^{-1} even after 150 cycles, corresponding to a high energy density of 365 Wh kg^{-1}. The above two research outcomes not only demonstrate that a high N-doping level could effectively increase active sites, but also demonstrated that pyridinic N might be in the best doping position to benefit the electrochemical performance compared with pyrrolic N and quaternary N dopants. In addition, elemental N doped, elemental phosphorus was also introduced to enhance the K^+ adsorption ability and regulate the electronic properties.[62] Guo et al. prepared 3D honeycomb-like architecture N, P-codoped carbon (Figure 5d), which shortened the K ions diffusion length and enhanced the ionic kinetics.[63] Taking into consideration the structural design for porous carbon, Guo et al. reported that amorphous ordered mesoporous carbon (OMC) could function as a good anode for high-performance PIBs.[64] The as-prepared amorphous OMC presented two broad peaks at around 23° and 44 and showed a microflake morphology with a diameter of 500–800 nm (Figure 5e). Due to the large surface area of OMC flakes, surface storage mainly charged the capacity contribution, which would explain the phenomenon of high capacity at well above the potassiation potential over 0.5 V. The pseudocapacitance could lead to superior long-term cyclability of around 150 mAh g^{-1} at 1 A g^{-1} after 1000 cycles, corresponding to a capacity fading of only 0.03 % per cycle. Ma et al. proposed an "order-in-disorder" synergetic engineering strategy by in situ embedding nanographitic in the defective carbon structure.[65] Due to the porous and hollow carbon architectures built from interconnected carbon skeletons, the as-prepared anodes delivered high specific capacities of 328 mAh g^{-1} at 0.2 A g^{-1} and 161 mAh g^{-1} at 4 A g^{-1} with ultralong cycling stability over 2000 cycles at 1 A g^{-1}. As revealed by DFT calculations very recently that potassium ion adsorbability was increased in the order of N-doping, O-doping, and vacancy defects.[69] An ultra-high pyrrolic/pyridinic-N doped necklace-like hollow carbon (NHC) (Figure 5f) was prepared, which exhibited a high reversible specific capacity and outstanding rate capability (204 mAh g^{-1} at 2000 mA g^{-1}). As we mentioned above, hierarchically 3D carbon could facilitate ion kinetics and electron transport. Zhao et al. designed hierarchically porous interconnected carbon sheels by using metal–organic framework-based strategy, which obtained S, N-codoped carbon shells (Figure 5g). Benefiting its unique structure, the cell delivered an ultra-high-rate capability of 169 mAh g^{-1} at 32000 mA g^{-1}. Numerous cases demonstrated that the amorphous-feature carbon could be beneficial for cycling stability and rate capability. However, the large pesoducapacitance contribution would generally lead to a very slope discharge/charge curves as shown in Figure 5h. The majority capacity contribution above 0.5 V for anodes will lead to decrease the energy density for the full-cell design. Besides, the low Coulombic efficiency in the first few cycles might be due to the formation of the SEI layer on the large specific area of porous carbon.

Since the first discovery that nitrogen-doped vertically aligned carbon nanotube arrays could act as good electrocatalysts,[70] heteroatom-doping has been widely used as an effective strategy to improve the electrochemical performance via the introduction of active sites and electronic structure.[12b,62,71] For example, the above-mentioned N-doped hard carbon microsphere and carbon fiber electrodes both could deliver ultra-long cycling performance and a high-rate capability. In addition to nitrogen doping, S,[72] O,[53] P,[56] and F[73] doping were all adopted as having future prospects for improved electrochemical performance and also relied on simultaneous co-doping with various heteroatoms. With the different doping contents and species, the electronic interactions between the doping elements and the carbon matrix could generate synergistic effects, thus promoting high-performance batteries.

In view of the capacity contribution arising from the redox pseudocapacitance, their excellent rate performance and large specific capacity offer a competitive advantage

compared to the K-GIC reaction mechanism. The carbon fibers and porous carbon inherit the benefits of the soft carbon and possess larger interlayer spacing compared to highly crystalline graphitic carbon, which could accommodate more K ions and further adapt to the volume changes during potassiation/de-potassiation.

As discussed above, the research and development of PIBs have run basically along the lines of LIB and post Li-ion technologies. Representative carbon-based electrode materials with their preparation methods and electrochemical performance are listed in Table 1.

3. Dual ion batteries based on co-intercalation mechanisms

Although carbon-based anode materials have attracted considerable attention owing to their excellent stability and high-rate capability, potassium ion full batteries still face serious challenges related to fast capacity fading and poor rate performance, which have impeded their potential applications. Recently, owing to the staggering recent advances in carbon-based materials and aluminium-graphite capacitors, dual-ion batteries (DIBs) have been discovered that work on the basis of potassium-based electrolyte in combination with the co-intercalation mechanism of carbon.[98]

Since 2014 and 2015, dual-graphite batteries have enabled researchers to realize ion intercalation under high voltage.[28a,99] Emerging research efforts have demonstrated that co-intercalation reactions take place where ions and the ion solvent intercalate into the layered host materials. These ion intercalations could break the thermodynamic and kinetic limits for energy storage. For example, it has been demonstrated that the constraints of Na storage in graphite could be broken by the introduction of ether-based solvents.[100] In the case of PIBs, it has been demonstrated by Pint et al. that the electrochemical co-intercalation of K ions into graphitic materials is capable of exhibiting long-term durability and high rate capability in diglyme and monoglyme electrolytes.[75] The co-intercalation reaction mechanism shares similarities with non-faradaic super capacitance behaviour,[101] which relies on the weak ion-host interaction mediated by a solvent shell, especially for the small Stock radius of K ions.[102] Therefore, this reaction mechanism could offer fast ionic transportation and enable high-rate capabilities.

On the basis of this working principle, the first potassium-based DIB device was proposed by Placke et al. (Figure 6a).[103] In combination with an ionic liquid (IL)-based electrolyte, this DIB technology built on dual-graphite batteries (DGBs) results in a high operating voltage potential over 4.5 V and reasonable specific capacity over 40 mAh g^{-1} with coulombic efficiency >99 %, indicating excellent reversibility. After 1500 cycles, a high-capacity retention ratio of 95 % could be achieved, which further demonstrated its stability during cycling. Lu et al. also used graphite as both anode and cathode to test the electrochemical performance in conventional KPF_6 based electrolyte (Figure 6b). The proposed K^+/PF_6^- co-insertion DGBs exhibited higher potassiation capacity of over 60 mAh g^{-1} with an operating voltage of 3.95 V compared with the previous reports.[104] To improve the electrochemical performance and regulate the operating voltage, Tang et al. used expanded graphite as cathode and mesocarbon mi-

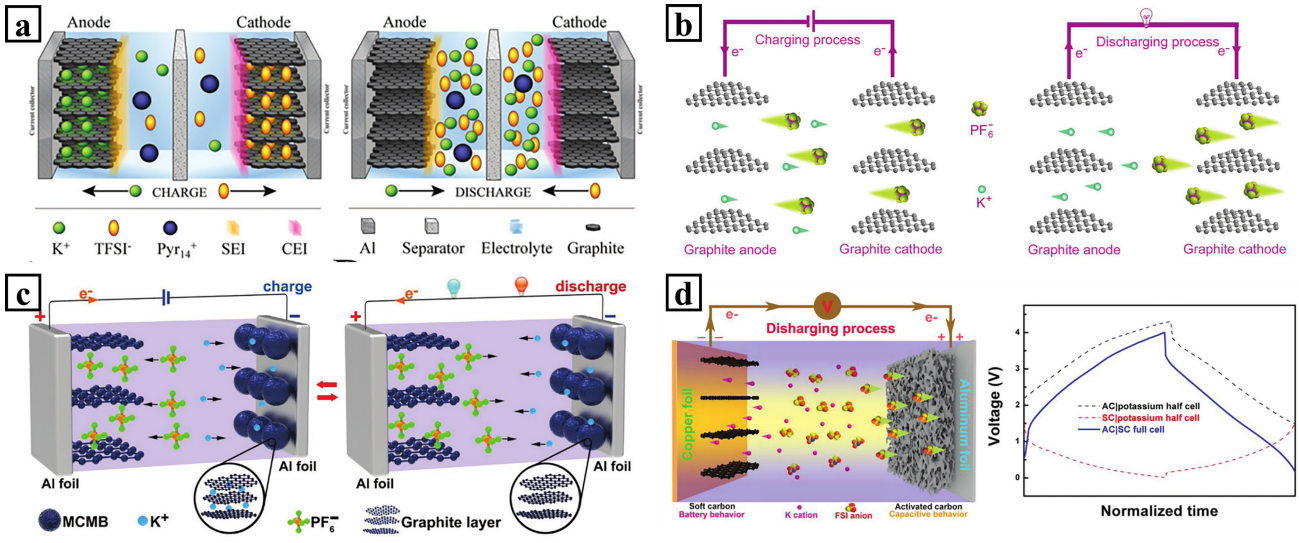

Figure 6. Schematic illustration of the PDIBs configuration. a) Symmetric graphite electrodes in combination with a potassium-containing ionic liquid electrolyte.[103] Reprinted from Beltrop et al., with permission. Copyright © 2017, Royal Society of Chemistry; b) Symmetric graphite electrodes in 0.8 M KPF_6 electrolyte.[106] Reprinted from Lu et al., with permission. Copyright © 2017, John Wiley and Sons; c) Graphite as cathode and mesocarbon microbead (MCMB) as the anode in KPF_6 electrolyte.[105] Reprinted from Tang et al., with permission. Copyright © 2017, John Wiley and Sons; d) Battery-supercapacitor hybrid device (BSH) and normalized voltage-time curves.[107] Reprinted from Lu et al., with permission. Copyright © 2018, John Wiley and Sons.

Table 1: Summary of representative carbon-based electrode materials.

Materials	Cycling performance[a]	Rate capability[b]	Refs.
Commercial graphite	100 (50) @ 0.7 C	80 @ 1 C	[26]
Polynanocrystalline graphite	75 (300) @ 0.5 C	13.6 @ 5 C	[31]
Expanded graphite	228 (200) @ 0.25 C	175 @ 1 C	[35]
Activated graphite	100.3 (100) @ 1 C	30 @ 5 C	[2c]
Graphite in EC:PC electrolyte	220 (200) @ 0.1 C	50 @ 1 C	[33]
Pencil-trace	200 (350) @ 2 C	110 @ 5 C	[74]
Soft carbon (Pyrolyzed PTCDA)	170 (50) @ 2.8 C	140 @ 7 C	[26]
Hard carbon microspheres	216 (100) @ 0.14 C	136 @ 7 C	[47]
Hard-soft carbon composites	186 (200) @ 1.4 C	190 @ 2.8 C	[55]
Multi layered graphene in glyme-based electrolytes	95 (1000) @ 10 C	80 @ 50 C	[75]
F-doped few-layer graphene	**165.9 (200) @ 2.5 C**	**212.6 @ 2.5 C**	**[73]**
N-doped few-layer graphene	210 (100) @ 0.5 C	50 @ 1 C	[76]
N-doped graphene	320 (60) @ 0.25 C	170 @ 2.5 C	[77]
N-doped porous carbon monolith	152 (3000) at 5 C	178 @ 25 C	[49]
N-doped carbon nanotubes	254.7 (300) @ 0.25 C	102 @ 10 C	[36]
N-doped hierarchically porous carbon	296.8 (100) @ 0.25 C	193.1 @ 2.5 C	[78]
N-doped carbon nanofibre	146 (4000) @ 10 C	101 @ 100 C	[61]
S-doped reduced graphene oxides	361 (50) @ 0.25 C	224 @ 5 C	[72]
N/O codoped hard carbon	130 (1100) @ 5.25 C	118 @ 15 C	[53]
P/O codoped graphene	160 (600) @ 10 C	165 @ 10 C	[56]
S/O codoped porous hard carbon	108.4 (2000) @ 5 C	158 @ 5 C	[51]
Nitrogen-rich hard carbon	180 (4000) @ 2.5 C	154 @ 100 C	[49]
Free-standing N-doped carbon nanofibre	179 (1900) @ 1.4 C	110 @ 14 C	[79]
Derived carbon from waste-tire Rubber	141 (200) @ 0.7 C	60 @ 2.8 C	[80]
Hollow carbon nanospheres	212 (100) @ 2.8 C	298 @ 0.14 C	[38]
Polycrystalline soft carbon semi-hollow microrods	249 (100) @ 0.5 C	100 @ 5 C	[56]
Porous carbon nanofiber paper	211 (1200) @ 6 C	140 @ 25 C	[60]
Graphitic carbon nanocage	195 (100) @ 0.28 C	175 @ 49 C	[40]
Short range order mesoporous carbon	146.5 (1000) @ 5 C	144.2 @ 5 C	[64]
N, S- co-doped thin carbon	65 (900) @ 10 C	64 @ 20 C	[68]
Graphite with high concentration electrolyte	255 (2000) 0.5 C	N/A	[81]
Nitrogen-doped hierarchical porous carbon	157 (12000) 10 C	94 @ 50C	[82]
Biomass porous carbon	247.8 (100) @ 0.5 C	152 @ 5C	[83]
Sub-micro carbon fibres @ carbon nanotubes	193 (300) @ 1.4 C	108 @ 7 C	[84]
N, P-codoped porous carbon	270.4 (1000) @ 5C	119.5 @ 50 C	[63]
Honeycomb hard carbon	67.6 (100) @ 2.5C	42 @ 16 C	[85]
Necklace-like nitrogen-doped hollow carbon	161.3 (1600) @ 5C	204.8 @ 10 C	[67]
Biomorphic N-doped carbon	242.5 (200) @ 0.5C	102.6 @ 10 C	[2g]
Coal-based carbon	118 (1200) @ 5C	88 @ 25 C	[86]
Hierarchically porous thin carbon shells	200 (4500) @ 80C	169 @ 160 C	[87]

Table 1: (Continued)

Pitch-derived soft carbon	200 (1000) @ 1.4 C	115.2 @ 7C	[24]
N-doped 3D mesoporous carbon nanosheets	321 (5000) @ 25C	106 @ 250C	[88]
Bubble-wrap-like carbon sheet with a rigid-flexible coupling porous	153 (5000) @ 10C	200 @ 25C	[89]
Sulfur-nitrogen rich carbon	125 (3000) @ 10C	72 @ 50C	[90]
Sulfur-grafted hollow carbon spheres	150 (1000) @ 15C	110 @ 25C	[91]
N/O dual doped hard carbon	189.5 (5000) @ 5C	178.9 @ 25C	[54]
Honeycomb-like N-doped carbon	143 (2000) @ 5C	103.1 @ 50C	[92]
Bi-heteroatom 3D porous carbon nanosheets	208 (6000) @ 10C	107 @ 100C	[93]
N-doped hierarchical dual-carbon	151.4 (6000) @ 25C	194 @ 25C	[94]
Graphdiyne framework	180 (2000) @ 5C	150 @ 25C	[95]
Expanded graphitic onion-like carbon	275 (1000) @ 2C	218 @ 5C	[32]
Hexagonal nano/microrods porous carbon	150.7 (400) @ 12.5C	187.5 @ 25C	[96]
Carbon dots with Ni/Co LDH hollow nanocages	188 (8000) @ 5C	N/A	[97]
N, P-codoped hollow carbon nanofibers	294.6 (3250) @ 10C	244.4 @ 40C	[39]
Crystalline lattice modified hard carbon	**283 (100) @ 0.25C**	**200 @ 0.5C**	**[48]**
N, O-codoped yolk-shell carbon sphere	189.2 (2500) @ 2.5C	183.3 @ 5C	[52]
N, S-codoped porous carbon	198 (2000) @ 10C	178@ 20C	[65]
N, O-codoped carbon nanobowls	178 (2000) @ 10C	154.8 @ 50C	[69]

[a] The cycling data are summarized as final capacity after (certain cycles) @ corresponding rate, and the unit of capacity is $mAh\,g^{-1}$. [b] The rate capability is summarized as retained capacity @ corresponding rate ($1C = 200\ mAh\,g^{-1}$).

crobead (MCMB) as the anode to construct DIB configurations (Figure 6c).[105] With the medium discharge voltage stabilized at 4.5 V, which is the highest among reported DIBs, the cell could deliver a high reversible capacity of over 60 $mAh\,g^{-1}$ at 100 $mA\,g^{-1}$.

Hybrid devices have been paid enough attention due to their competitive advantages from combining various systems.[93,108] With the benefits of high-energy-density PIBs and the merits of high-power-density supercapacitors, Lu et al. proposed a low-cost battery-supercapacitor hybrid (BSH) device based on soft carbon as anode and activated carbon as a cathode (Figure 6d).[107] As discussed in section 2.2, soft carbon features the advantage of high specific capacity with large interlayer spacing. As a result, with its combination of the battery behaviour of its soft carbon anode and the capacitive behaviour of its activated carbon cathode, this hybrid device can deliver high energy density of 120 $Wh\,kg^{-1}$ and a power density of 599 $W\,kg^{-1}$. Hence, it shows great promise as a good alternative to commercial lithium-ion batteries (energy density of 100–260 $Wh\,kg^{-1}$ and power density of 250–340 $W\,kg^{-1}$).

The development of DIBs is facing big challenges, though showing great promise to meet the requirements of high-operating voltage and high-power density devices. It is necessary to adopt various carbon-based materials for the development of DIBs. The anodic/cathodic reaction mechanisms should be further deeply understood and other alternative anodic ions might be potential candidates for co-insertion with K^+.

4. Other K–X ($X = O_2$, CO_2, S, Se, I_2) systems

The developments of next-generation stationary energy storage systems require high energy density and high power density.[109] In the past few years, lithium metal as anodes attracted numerous interests due to the high theoretical specific capacity (3860 $mAh\,g^{-1}$), low density (0.534 $g\,cm^{-3}$), and low electrochemical potential (−3.04 V vs. E^0).[110] As expected, potassium metal as anodes is also deserved to be paid enough attentions which are essential to develop low-cost with high theoretical capacities and energy densities devices. The current advanced state-of-the-art cathodes of K–X systems generally employed O_2,[111] CO_2,[112] S/Se,[113] and I_2[114] as cathode materials. The reversibility of the discharge/charge processes is essential to improve the energy efficiency of K–X systems. For instance, potassium carbonate will be generated after a discharged process for K-CO_2 batteries.[112] The decomposition process of K_2CO_3 would be needed to involve electrocatalysts. However, the electrochemical performance of K-CO_2 batteries hasn't been reported until now, which is possibly due to the difficult operation conditions of K metal and excellent catalysts. Since 2009, Dai and his co-worker demonstrated that carbon-based materials can effectively act as good electrocatalysts.[70] Numerous subsequent studies have paid attention to improving the catalyst properties, including tuning heteroatom doping,[13b] regulating carbon structure, introducing defects, to name a few.[16b,115] Along this research line, it is necessary to design carbon-based catalysts to

enable the concept of K-CO_2 batteries. For K-O_2 batteries, carbon can be a good matrix to enable fast electron transport and maintain good structural stability to support the ion kinetics, although Wu et al. have demonstrated it might not need catalysts to decompose the potassium superoxide.[3a] For K–S batteries, carbon matrix can enhance the electrical conductivity of the electrode materials, buffer the volume variations during cycling and alleviate the solutions of polysulfide.[116] Therefore, carbon-based electrode materials also attracted certain interests to explore the possibility for K–X systems.

Li-O_2 batteries have attracted significant attention due to their notably high theoretical energy density (3500 W h kg^{-1} based on Li_2O_2). Nevertheless, the asymmetric reaction mechanism due to the disproportionation reaction of LiO_2 into Li_2O_2 and O_2 during the discharge process and the direct oxidation of Li_2O_2 into O_2 during the charging process led to a high overpotential and low round-trip energy efficiency. Hence, it is necessary to study the one-electron redox process ($O_2 + e^- + M^+ \rightarrow MO_2$) for alternative Li-$O_2$ chemistry. In 2013, Wu et al. first introduced the concept of K-O_2 chemistry (Figure 7a)[117] with symmetric reactions and low overpotential based on the thermodynamically stable product KO_2. In addition, K-O_2 batteries offer the opportunity to eliminate the need for electrocatalysts, with a small potential gap of around 50 mV, which is the lowest among all the reported metal-oxygen batteries.[3a] The formation and subsequent oxidation of K_2O_2 triggered by the irreversible cell chemistry was responsible for capacity decay in K-O_2 batteries, which was demonstrated by X-ray photoelectron spectroscopy (APXPS).[118] In addition, the common impurities in the air such, as H_2O and CO_2 could reduce the chemical reversibility of ORR and OER in ionic liquid-based air batteries. In the past few years, pioneering work has been done to understand superoxide reactions and promote the long-term cycling stability of K-O_2 batteries through the regulation of salt chemistry and solvents to passivate the surface of K metal as the anode side. Indeed, tuning the electrolyte composition may help to form a uniform SEI layer, thus improving the cycling performance.[3b,c,111,119]

Although K-O_2 chemistry does not need to use electrocatalysts to lower the overpotential, carbon is still necessary as a host for the nucleation and growth of superoxide. The long-term stability of KO_2 is subject to question as to whether superoxide could be stable toward the electrolyte and the carbon cathode. In addition, the size and the morphology of the KO_2 formed on the carbon cathode side could block the penetration of oxygen species and the concentration of O_2^-, thus limiting the reaction kinetics and the rate performance.

Li-CO_2 as a new member of this battery family, has attracted attention because Li_2CO_3 ($\Delta_f G^o(Li_2CO_3) = -1132.12\ KJ/mol$) is more chemically stable than Li_2O_2 ($\Delta_f G^o(Li_2O_2) = -285.6\ KJ/mol$), where $\Delta_f G^o$ is the Gibbs free energy.[120] A proof of concept for K-CO_2 battery has recently been revealed via an aberration-corrected environmental transmission electron microscope (AC-ETEM).[112] During discharge, the formation of K_2CO_3 could be written as $2K^+ + 2e^- + 2CO_2 \rightarrow K_2CO_3 + CO$, and the charging process could be translated as $2K_2CO_3 + C \rightarrow 3CO_2 + 4K$. Our group has recently em-

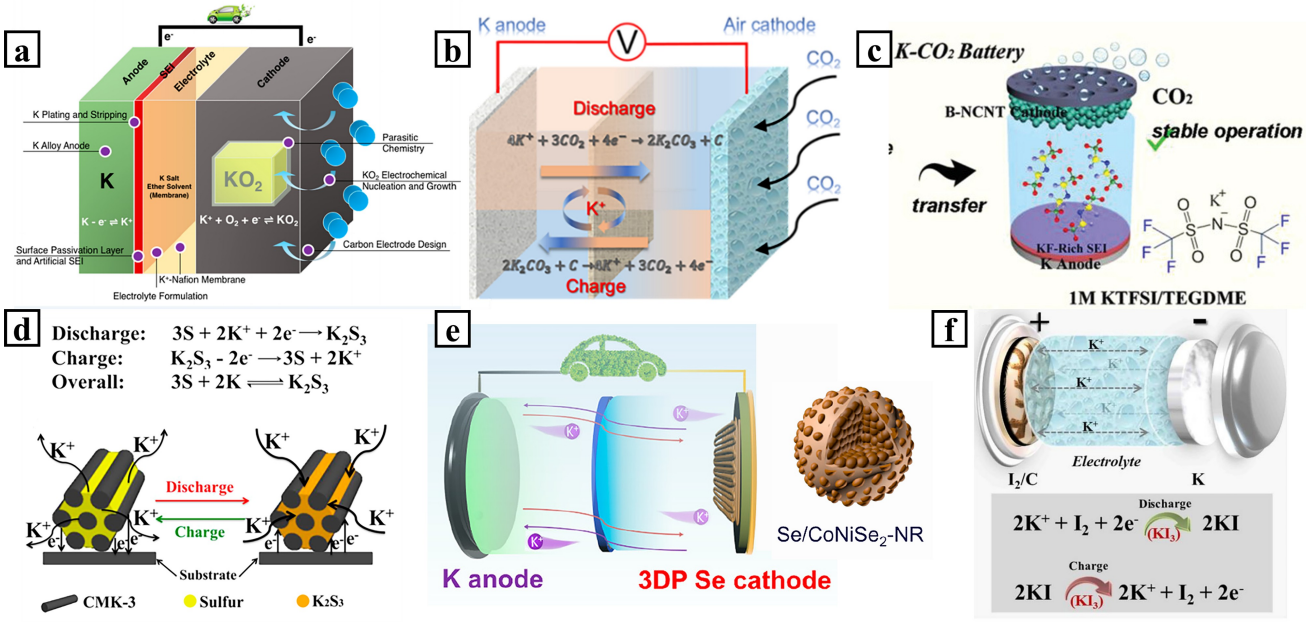

Figure 7. Schematic diagram of rechargeable battery systems. a) K-O_2.[117] Reprinted from Xiao et al., with permission. Copyright © 2018, American Chemical Society; b) K-CO_2.[121] Reprinted from Dai et al., with permission. Copyright © 2020, John Wiley and Sons, c) K-CO_2.[122] Reprinted from Qi et al., with permission. Copyright © 2021, John Wiley and Sons; d) K–S[5b] Reprinted from Zhao et al., with permission. Copyright © 2014, American Chemical Society; e) K–Se.[124] Reprinted from Yu et al., with permission. Copyright © 2020, John Wiley and Sons and f) K-I_2[114] batteries. Reprinted from Lu et al., with permission. Copyright © 2019, Elsevier Ltd.

ployed a novel bifunctional metal-free 3D porous carbon electrocatalyst for CO_2 reduction and evolution. The obtained K-CO_2 batteries (Figure 7b) showed high reversibility over 1500 h, which opens avenues for the rational design and development of cost-effective metal-CO_2 batteries with a high energy density and long cycle life.[121] In light of this work, Li et al. fabricated a high-performance K-CO_2 battery using passivated K anodes with artificial surface film and N-doped carbon nanotubes cathodes (Figure 7c),[122] which shows a high specific full discharge capacity (9436 mAh g^{-1}), small overpotential gap (0.81 V at 50 mA g^{-1}), and long cycle life (450 cycles or 3100 h with a curtailing capacity of 500 mAh g^{-1}).

Potassium-sulfur (K–S) batteries (Figure 7d) are emerging as another promising candidate for developing high-energy density systems.[5b,123] There are two main concerns: a) Li–S batteries, potassium-polysulfide dissolution, and the related shuttle reactions, and b) the low utilization ratio due to the reactive potassium surface.[5c] Encapsulating sulphur into a carbon matrix is a common way to address the above concerns.[125] So far, ordered mesoporous carbon (CMK-3),[5b] sulfurized polyacrylonitrile (SPAN),[5c] and three-dimensional free-standing carbon nanotube (3D-FCN)[5a] have been adopted as potential cathodes for electrochemical testing in K–S batteries. Unlike the formation of Li_2S in the Li–S systems, it was demonstrated that K_2S_3 could be the final discharge product for K–S conversion processes.[5b] More recently, self-supported SeS_2 in the nitrogen-doped free-standing porous carbon has been reported that it could deliver a high reversible capacity of 417 mAh g^{-1} after 1000 cycles with 85 % capacity retention at 0.5 A g^{-1}, which is attributed to the interconnected porous carbon structures thus facilitating the ions/electrons transportations.[116] Ding et al. developed a Se and $CoNiSe_2$ coembedded nanoreactor (Se/$CoNiSe_2$-NR) affording low carbon content as cathodes,[126] which show relatively stable cycling stability with a capacity decay rate of 0.038 % per cycle over 950 cycles at 1.0 C. Inspired by the research history of LIBs, the small-molecule Se embedded in freestanding N-doped porous carbon nanofibers thin film (Se@NPCFs) was fabricated. The generation of polyselenides (K_2Se_n, $3 \le n \le 8$) was effectively suppressed by electrochemical reaction dominated by Se_2 molecules, thus significantly enhancing the utilization of Se and effecting the voltage platform of the K–Se battery (Figure 7e).[124] So far, the cycling and rate performance is far below expectations, and further experimental results are needed to validate the feasibility of this new class of systems.

K-O_2 typically needs an open system which brings more complicated circumstances, and K–S may need to be further explored to improve the cycle life and performance. Recently, another conversion-type reaction, namely, potassium-iodine (K-I_2) (Figure 7f) was established based on a high conversion voltage of 3 V and iodine/triiodide redox reactions.[114] By employing a free-standing I_2/Carbon composite as cathode, the I_2/I_3^- and I_3^-/I^- redox couples offered a high capacity (156 mAh g^{-1}) and stable cycling life (71 % capacity retention after 500 cycles).

The above four conversion-type reactions have opened up a new avenue to explore new types of potassium storage systems. It should be noted that the cathode side basically needs to include carbon-based host materials. Therefore, it is still worth exploring various functional porous carbon hosts to improve the charge-transfer capability and increase the solvation of K^+ in the electrolyte. On the other hand, the direct use of K metal may lead to huge concerns about dendritic growth and severe side reactions. In K-O_2 systems, some intermetallic alloys, such as K_3Sb as counter anode[127] and liquid Na–K alloy,[113] were employed to mitigate non-uniform plating and dendrite growth problems.

5. Carbon as host for metal protection

Metallic potassium was deemed as a desirable anode for potassium-ion batteries due to its low electrochemical potential (−2.93 V vs. SHE), high theoretical capacity (687 mAh g^{-1}), and large abundance (≈0.0017 wt %).[128] Nevertheless, like the issues of lithium metal anodes, the high reactivity, uncontrollable dendritic growth, large volume changes, unstable interface, and intricate side reactions hampered its further development and practical application.[129] Employing carbon-based material as a matrix for metal protection is an effective strategy to achieve dendrite-free K metal anodes.[130] In the past, aligned carbon nanotube membrane (ACM),[131] reduced graphene oxide,[132] and amine functionalization of the carbon scaffolds[133] were fabricated for constructing dendrite-free, good wettability, processable, and moldable metal anodes (Figure 8a). A graphite-intercalation-compound (GIC) through simple high-temperature stirring was employed to fabricate scaffold for K-GIC anodes,[128a] which exhibited environmental stability in air/water and excellent cycling stability (Figure 8b). The optimized interlayer insertion/extraction and reduced affinity energy of K can suppress dendrite growth and alleviate volume expansion of as-prepared material, resulting in excellent electrochemical performances. Therefore, it suggests that the promising graphite protection foundation knowledge and technologies already available for Li-metal could be applied to K-metal anode. So far, liquid Na–K alloys benefited from low viscosity like "liquid",[134] high surface tension, and electronic conductivity like "metal", which delivered stable high capacity and could not grow dendrites (Figure 8c).[135] Yuan et al., constructed semi-solid K metal electrodes with rich C–K bonds by in situ replacement of N-doped carbon nanotubes (CNT) and liquid Na–K alloy,[136] which could deliver higher stability with dendrite-free. Based on the theoretical calculation (Figure 8d), pyrrolic-N and pyridinic-N reacted spontaneously with the NaK alloy cluster at the wall of the carbon nanotube, accelerating the removal of N atoms. With the replacement of these graphite-N by NaK clusters, a large number of defects were produced and the NaK-CNT structure was employed as the main C–K bond due to its high content (74.32 %), optimizing the activity of Na–K alloy raised to ≈90 %. Besides, tailoring current collector as metal protection attracted numerous interests due to the

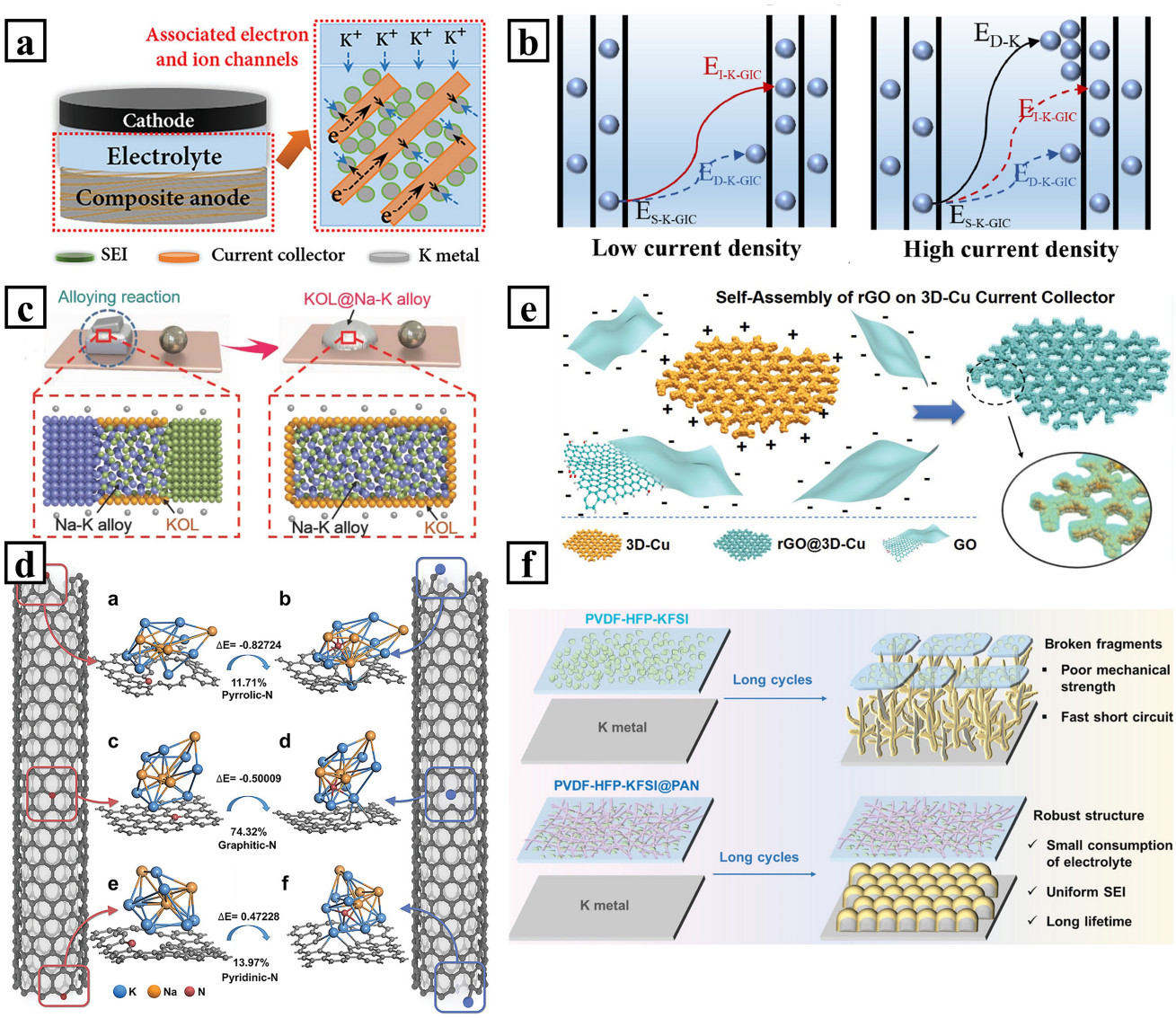

Figure 8. a) Schematic diagram of K metal protection (K-ACM).[131] Reprinted from Yang et al., with permission. Copyright © 2019, John Wiley and Sons; b) mechanisms of K^+ stripping/depositing of K-GIC.[128a] Reprinted from Zhang et al., with permission. Copyright © 2021, Elsevier Ltd.; c) Schematic illustration of KOL@Na–K alloy.[135] Reprinted from Tu et al., with permission. Copyright © 2018, John Wiley and Sons; d) Theoretical calculations of graphitic-N replacement with NaK alloy.[136] Reprinted from Zhang et al., with permission. Copyright © 2022, John Wiley and Sons; e) Self-assembly of rGO@3D–Cu current collector.[139] Reprinted from Mitlin et al., with permission. Copyright © 2019, John Wiley and Sons; f) Schematic illustration of the electrochemical deposition behaviours of K metal using PVDF-HFP-KFSI and PVDF-HFP-KFSI@PAN CGPE.[140] Reprinted from Liu et al., with permission. Copyright © 2022, John Wiley and Sons.

relatively stable metal plating-stripping behavior.[137] For instance, an oxygen-rich treated carbon cloth (TCC) was designed as the K plating host to guide K homogeneous nucleation and suppress the dendrite growth.[138] Liu and co-workers synthesized a functionalized 3D copper current collector (rGO@3D–Cu) with reduced graphene oxide, which achieved abundant potassiophilic surface, low nucleation barrier, high specific surface area and porous structure (Figure 8e).[139] As expected, the as-prepared metal anodes achieved a unique synergy driven by interfacial tension and geometry, the symmetric rGO@3D–Cu cells exhibit stable cycling at 0.1 mA cm^{-2} and the half-cells are stable at 0.5 mA cm^{-2} for 10000 min. More recently, Zhang and co-workers developed a robust composite gel polymer electrolyte (CGPE),[140] which was effective in regulating K stripping/plating and enabling stable K metal anode (Figure 8f). The as-prepared K metal symmetrical cells with CGPE exhibit a long cycle life over 1200 h at the current density of 0.5 mA cm^{-2}. The introduction of PAN nanofibers not only improved the mechanical properties, but also widened the electrochemical stability window.

To date, a stable SEI layer formation upon the K metal anode has been considered as a crux to ensure battery performance. However, the nonuniform stripping and deposition of K ions caused huge volumetric change on the K anode, which led to the growth of K dendrites and SEI layer

fracture. The research on the use of carbon as host for K-metal anode protection was still at the very beginning stage, although it might possibly learn from the studies of Li and Na metal anodes. Moreover, the plating and stripping behaviours of carbon-based "host" for stable K metal were still in debate, and more delicate studies on electrolytes were still limited.

6. Outlook and Perspectives

Over the past few years, notable progress has been made in the development of carbon-based potassium-ion storage devices, and it should be noted that various carbon-based materials have been realized to address/solve the practical problems impeding multifunctional applications, such as high-energy-density and high-power-density devices for energy storage. Nevertheless, several key challenges related to electrode materials and technologies need to be addressed for future research directions.

Intrinsic and assembled structure evaluation and regulation are the key to addressing the above issues while PIBs move towards practical applications in the future. In particular, graphite-based electrode materials exhibit low but safe working voltage potential (below the dendrite formation potential) for high-energy-density PIBs. One of the major challenges is to design high ordered architecture to allow potassium ion storage, and also serve as a stable host for volume variations during discharge/charge processes. As for hard and soft carbon-based materials, they deserve to be further studied due to their excellent rate performance and ultra-stable cycling performance due to the contribution of pseudocapacitance. There is still a major obstacle, however, arising from their low theoretical capacity, especially due to the large atomic size and weight of K^+. It was demonstrated that heteroatom-doping is an effective strategy to improve the electrochemical performance via the introduction of active sites and regulating the intrinsic electronic structure. Although the high specific capacity and ultra-long cycling performance have been achieved via doping with various elements, the functions of each doping element still need to be deeply understood, especially for S, O, and P. In addition, the doping levels of elements still need to be determined by further experimental evidences.

To alleviate the shortcomings of low coulombic efficiency and continuous electrolyte consumption for SEI formation, one effective method is to optimize the electrolyte composition to suppress the reduction of electrolytes and avoid side reactions. Taking account of the aspect of the carbon-based materials themself, it should be noted that a large surface area is considered to have pros and cons, which could increase the contact between the active materials and electrolytes to facilitate electron/ion transportation, while creates more interfaces to consume the electrolyte in forming the SEI. In this context, it is best to develop a suitable pore structure with moderate surface area (avoid the formation of excessive microporous), which will facilitate the transportation of ions/electrons to maintain the integrity of the electrodes and avoid overconsumption of the electrolyte to increase the coulombic efficiency during cycling.

As the most reactive element compared to Li and Na, the surface of K deserves to be paid great attention. The simultaneous problems brought by the developments of K–X ($X = CO_2$, O_2, S, Se, I_2) batteries involve the active K metal as the counter anode. When approaching practical application, some serious problems emerge: a) poor K plating/stripping, b) electrolyte reduction on the K surface, and c) K dendrite formation and safety concerns. Inspired by the abundance of research on lithium metal anode,[141] it is promising to use thin layer carbon in such forms as a reduced graphene oxide layer[142] as a benign host to protect the active K metal and avoid the concern about dendrites.

It has been realized that DFT calculations are effective tools to help understand K-ion insertion/de-insertion chemistry. For instance, DFT calculations have been successfully applied to predict that carbon-based electrode materials like hexagonal BC_3[143] and B-doped graphene,[43b] could be potential anode materials with high theoretical capacity, fast ion kinetics for transportation, and long-term cycling performance. In the future, a deep understanding of these electrode materials, including their reaction kinetics, interfacial reactions, and K ion intercalation chemistry during cycling, is needed, based on enough experimental evidence in association with theoretical calculations and reasonable guidance.

The availability of hybrid devices offers more opportunities for the development of new, low-cost, and high-power-density devices. In principle, sluggish redox processes in battery-type electrodes hinder their potential application in high-power devices, while the low energy density of supercapacitors is the key limitation to their application in future electrical cars and smart energy-related devices. Therefore, the low-cost BSH devices are highly desirable as their high power density, approaching conventional supercapacitors with proper battery-electrode architecture design,[144] it is desirably to prepare highly mesoporous conductive carbon with an increased active surface area to accommodate ions but enhance the surface redox reactions via specific heteroatom doping. After a decade's research, the main obstacle is still their limited low operating voltage window, it is expected that advanced carbon electrodes with an appropriately designed architecture could be developed to match the counter electrode in configurations that could deliver high specific capacity, and thus leading to high-energy-density devices.

An effective K-ion SEI layer formation is regarded as a key role to stabilize the plating/stripping behaviours of potassium metal and cripple intricate side reactions at K-metal/electrolyte interface.[145] However, the K-ion SEI is still unascertainable, which is partly because the unclear mechanism of the Fermi level and the unoccupied molecular orbital.[146] Moreover, the cations in the electrolytes under various energy storage devices lead to huge differences in the K-ion SEI formation in terms of the chemical composition, morphology, structure, and mechanical stability. Hence, it would be necessary to focus on the protection and

modification of K-metal anode that can realize the significance of constructing a stable K-ion SEI layer, which must be established on the great chemical environment difference in various K-metal based energy storage device. For constructing safe and long-life K metal batteries with features of high-operating voltage, high-stability, and high-power density, it should be the ultimate goal to study the discrepant mechanism and structure-function relationship between various carbon-based hosts with K-metal anode SEI layer in the future.

A wide range of carbon-based potassium storage devices are being realized for potential application in large-scale energy storage. Continued research and development are being encouraged to overcome the above major hurdles and target the goals of low cost, long life, and high safety to create more reliable energy storage systems.

Acknowledgements

This work was financially supported by the National Natural Science Foundation of China (Grant No. 52104315), Foundation for Innovative Research Groups of the National Natural Science Foundation of China (No. 52121004), Australian Research Council (DP210101486, FL190100126, and DP200101862). Open Access publishing facilitated by The University of Adelaide, as part of the Wiley - The University of Adelaide agreement via the Council of Australian University Librarians.

Conflict of Interest

The authors declare no conflict of interest.

Data Availability Statement

Data sharing is not applicable to this article as no new data were created or analyzed in this study.

Keywords: Anode · Carbon Materials · Dual-Ion Batteries · K-Metal · Potassium-Ion Storage

[1] a) Y. Liu, Z. Tai, J. Zhang, W. K. Pang, Q. Zhang, H. Feng, K. Konstantinov, Z. Guo, H. K. Liu, *Nat. Commun.* **2018**, *9*, 3645; b) G. He, L. F. Nazar, *ACS Energy Lett.* **2017**, *2*, 1122–1127; c) W. Zhang, Y. Liu, Z. Guo, *Sci. Adv.* **2019**, *5*, eaav7412; d) W. Zhang, J. Mao, S. Li, Z. Chen, Z. Guo, *J. Am. Chem. Soc.* **2017**, *139*, 3316–3319.

[2] a) W. Zhang, W. K. Pang, V. Sencadas, Z. Guo, *Joule* **2018**, *2*, 1534–1547; b) J. Zheng, W. Deng, Z. Hu, Z. Zhuo, F. Liu, H. Chen, Y. Lin, W. Yang, K. Amine, R. Li, *ACS Energy Lett.* **2018**, *3*, 65–71; c) Z. Tai, Q. Zhang, Y. Liu, H. Liu, S. Dou, *Carbon* **2017**, *123*, 54–61; d) Y. Liu, F. Fan, J. Wang, Y. Liu, H. Chen, K. L. Jungjohann, Y. Xu, Y. Zhu, D. Bigio, T. Zhu, C. Wang, *Nano Lett.* **2014**, *14*, 3445–3452; e) W. Wang, J. Zhou, Z. Wang, L. Zhao, P. Li, Y. Yang, C. Yang, H. Huang, S. Guo, *Adv. Energy Mater.* **2018**, *8*, 1701648; f) Y.-S. Xu, S.-Y. Duan, Y.-G. Sun, D.-S. Bin, X.-S. Tao, D. Zhang, Y. Liu, A.-M. Cao, L.-J. Wan, *J. Mater. Chem. A* **2019**, *7*, 4334–4352; g) C. Gao, Q. Wang, S. Luo, Z. Wang, Y. Zhang, Y. Liu, A. Hao, R. Guo, *J. Power Sources* **2019**, *415*, 165–171; h) W. Zhang, Z. Wu, J. Zhang, G. Liu, N.-H. Yang, R.-S. Liu, W. K. Pang, W. Li, Z. Guo, *Nano Energy* **2018**, *53*, 967–974; i) L. Li, W. Zhang, X. Wang, S. Zhang, Y. Liu, M. Li, G. Zhu, Y. Zheng, Q. Zhang, T. Zhou, W. K. Pang, W. Luo, Z. Guo, J. Yang, *ACS Nano* **2019**, *13*, 7939–7948; j) S. Liu, J. Mao, Q. Zhang, Z. Wang, W. K. Pang, L. Zhang, A. Du, V. Sencadas, W. Zhang, Z. Guo, *Angew. Chem. Int. Ed.* **2020**, *59*, 3638–3644; k) D. Wu, W. Zhang, Y. Feng, J. Ma, *J. Mater. Chem. A* **2020**, *8*, 2618–2626; l) M. Wu, J. Liao, L. Yu, R. Lv, P. Li, W. Sun, R. Tan, X. Duan, L. Zhang, F. Li, J. Kim, K. H. Shin, H. Seok Park, W. Zhang, Z. Guo, H. Wang, Y. Tang, G. Gorgolis, C. Galiotis, J. Ma, *Chem. Asian J.* **2020**, *15*, 995–1013; m) W. Zhang, H. Wang, N. Zhang, H. Liu, Z. Chen, L. Zhang, S. Guo, D. Li, J. Xu, *ACS Appl. Mater. Interfaces* **2019**, *11*, 29807–29813.

[3] a) X. Ren, Y. Wu, *J. Am. Chem. Soc.* **2013**, *135*, 2923–2926; b) W. Wang, N. C. Lai, Z. Liang, Y. Wang, Y. C. Lu, *Angew. Chem.* **2018**, *130*, 5136–5140; c) N. Xiao, G. Gourdin, Y. Wu, *Angew. Chem.* **2018**, *57*, 10864–10867.

[4] J. Wu, J. Liu, Z. Lu, K. Lin, Y.-Q. Lyu, B. Li, F. Ciucci, J.-K. Kim, *Energy Storage Mater.* **2019**, *23*, 8–16.

[5] a) J.-Y. Hwang, H. M. Kim, C. S. Yoon, Y.-K. Sun, *ACS Energy Lett.* **2018**, *3*, 540–541; b) Q. Zhao, Y. Hu, K. Zhang, J. Chen, *Inorg. Chem.* **2014**, *53*, 9000–9005; c) J.-Y. Hwang, H. M. Kim, Y.-K. Sun, *J. Mater. Chem. A* **2018**, *6*, 14587–14593.

[6] C. Liu, S. Luo, H. Huang, Z. Wang, A. Hao, Y. Zhai, Z. Wang, *Electrochem. Commun.* **2017**, *82*, 150–154.

[7] C. Yang, J. Feng, F. Lv, J. Zhou, C. Lin, K. Wang, Y. Zhang, Y. Yang, W. Wang, J. Li, S. Guo, *Adv. Mater.* **2018**, *30*, 1800036.

[8] L. Wang, J. Zou, S. Chen, G. Zhou, J. Bai, P. Gao, Y. Wang, X. Yu, J. Li, Y.-S. Hu, H. Li, *Energy Storage Mater.* **2018**, *12*, 216–222.

[9] F. Yuan, Z. Li, D. Zhang, Q. Wang, H. Wang, H. Sun, Q. Yu, W. Wang, B. Wang, *Adv. Sci.* **2022**, *9*, 2200683.

[10] C. Wei, Y. Tao, H. Fei, Y. An, Y. Tian, J. Feng, Y. Qian, *Energy Storage Mater.* **2020**, *30*, 206–227.

[11] a) see ref. [7]; b) J. Zhou, L. Wang, M. Yang, J. Wu, F. Chen, W. Huang, N. Han, H. Ye, F. Zhao, Y. Li, Y. Li, *Adv. Mater.* **2017**, *29*, 1702061; c) N. Xiao, W. D. McCulloch, Y. Wu, *J. Am. Chem. Soc.* **2017**, *139*, 9475–9478; d) Z. Huang, Z. Chen, S. Ding, C. Chen, M. Zhang, *Mater. Lett.* **2018**, *219*, 19–22; e) M. Mao, C. Cui, M. Wu, M. Zhang, T. Gao, X. Fan, J. Chen, T. Wang, J. Ma, C. Wang, *Nano Energy* **2018**, *45*, 346–352.

[12] a) X. Liu, L. Dai, *Nat. Rev. Mater.* **2016**, *1*, 16064; b) J. Zhang, Z. Zhao, Z. Xia, L. Dai, *Nat. Nanotechnol.* **2015**, *10*, 444–452; c) J. Li, Y. Wang, H. Song, Y. Guo, S. Hu, H. Zheng, S. Zhang, X. Li, Q. Gao, C. Li, Z. Zhu, Y. Wang, *Adv. Compos. Hybrid Mater.* **2023**, *6*, 83.

[13] a) J. Zhang, Z. Xia, L. Dai, *Sci. Adv.* **2015**, *1*, e1500564; b) W. Yang, J. Zhou, S. Wang, W. Zhang, Z. Wang, F. Lv, K. Wang, Q. Sun, S. J. E. Guo, E. Science, *Energy Environ. Sci.* **2019**, *12*, 1605–1612; c) C. Hu, J. Qu, Y. Xiao, S. Zhao, H. Chen, L. Dai, *ACS Cent. Sci.* **2019**, *5*, 389–408; d) R. Paul, L. Zhu, H. Chen, J. Qu, L. Dai, *Adv. Mater.* **2019**, *31*, 1806403.

[14] a) L. Dai, Y. Xue, L. Qu, H.-J. Choi, J.-B. Baek, *Chem. Rev.* **2015**, *115*, 4823–4892; b) X. Zhu, F. Xia, D. Liu, X. Xiang, J. Wu, J. Lei, J. Li, D. Qu, J. Liu, *Adv. Funct. Mater.* **2023**, *33*, 2207548.

[15] J. Choi, A. Jin, H. D. Jung, D. Ko, J. H. Um, Y. J. Choi, S. H. Kim, S. Back, S.-H. Yu, Y. Piao, *Energy Storage Mater.* **2022**, *48*, 325–334.

[16] a) H. Jiang, P. S. Lee, C. Li, *Energy Environ. Sci.* **2013**, *6*, 41–53; b) C. Hu, Y. Lin, J. W. Connell, H. M. Cheng, Y. Gogotsi, M. M. Titirici, L. Dai, *Adv. Mater.* **2019**, *31*, 1806128.

[17] a) F. Du, D. Yu, L. Dai, S. Ganguli, V. Varshney, A. Roy, *Chem. Mater.* **2011**, *23*, 4810–4816; b) Y. Xue, Y. Ding, J. Niu, Z. Xia, A. Roy, H. Chen, J. Qu, Z. L. Wang, L. Dai, *Sci. Adv.* **2015**, *1*, e1400198; c) J. Xu, M. Wang, N. P. Wickramaratne, M. Jaroniec, S. Dou, L. Dai, *Adv. Mater.* **2015**, *27*, 2042–2048; d) J. Shui, M. Wang, F. Du, L. Dai, *Sci. Adv.* **2015**, *1*, e1400129.

[18] Y. Wu, H. Zhao, Z. Wu, L. Yue, J. Liang, Q. Liu, Y. Luo, S. Gao, S. Lu, G. Chen, X. Shi, B. Zhong, X. Guo, X. Sun, *Energy Storage Mater.* **2021**, *34*, 483–507.

[19] a) X. Jiang, B. Song, D. Tománek, *Phys. Rev. Appl.* **2018**, *9*, 044015; b) J. Xu, Y. Dou, Z. Wei, J. Ma, Y. Deng, Y. Li, H. Liu, S. Dou, *Adv. Sci.* **2017**, *4*, 1700146; c) M. S. Dresselhaus, G. Dresselhaus, *Adv. Phys.* **2002**, *51*, 1–186; d) Y. Yang, B. Cheng, J. Yu, L. Wang, W. Ho, *Nano Res.* **2023**, *16*, 4506–4514.

[20] T. Xu, Y. Wang, Z. Xiong, Y. Wang, Y. Zhou, X. Li, *Nano-Micro Lett.* **2023**, *15*, 6.

[21] Y. y. Zhu, Y. h. Wang, Y. t. Wang, T. j. Xu, P. Chang, *Carbon Energy* **2022**, *4*, 1182–1213.

[22] H. Lei, J. Li, X. Zhang, L. Ma, Z. Ji, Z. Wang, L. Pan, S. Tan, W. Mai, *InfoMat* **2022**, *4*, e12272.

[23] J. Zhang, L. Lai, H. Wang, M. Chen, Z. X. Shen, *Mater. Today Energy* **2021**, *21*, 100747.

[24] Y. Liu, Y.-X. Lu, Y.-S. Xu, Q.-S. Meng, J.-C. Gao, Y.-G. Sun, Y.-S. Hu, B.-B. Chang, C.-T. Liu, A.-M. Cao, *Adv. Mater.* **2020**, *32*, 2000505.

[25] a) P. Ge, M. Fouletier, *Solid State Ionics* **1988**, *28*, 1172–1175; b) M. D. Slater, D. Kim, E. Lee, C. S. Johnson, *Adv. Funct. Mater.* **2013**, *23*, 947–958.

[26] Z. Jian, W. Luo, X. Ji, *J. Am. Chem. Soc.* **2015**, *137*, 11566–11569.

[27] W. Luo, J. Wan, B. Ozdemir, W. Bao, Y. Chen, J. Dai, H. Lin, Y. Xu, F. Gu, V. Barone, L. Hu, *Nano Lett.* **2015**, *15*, 7671–7677.

[28] a) S. Komaba, T. Hasegawa, M. Dahbi, K. Kubota, *Electrochem. Commun.* **2015**, *60*, 172–175; b) R. A. Adams, A. Varma, V. G. Pol, *J. Power Sources* **2019**, *410*, 124–131.

[29] K. Share, A. P. Cohn, R. E. Carter, C. L. Pint, *Nanoscale* **2016**, *8*, 16435–16439.

[30] H. Kim, J. C. Kim, M. Bianchini, D. H. Seo, J. Rodriguez-Garcia, G. Ceder, *Adv. Energy Mater.* **2018**, *8*, 1702384.

[31] Z. Xing, Y. Qi, Z. Jian, X. Ji, *ACS Appl. Mater. Interfaces* **2017**, *9*, 4343–4351.

[32] C. Meng, M. Yuan, B. Cao, Z. Jiang, J. Zhang, A. Li, X. Chen, M. Jia, H. Song, *J. Mater. Chem. A* **2022**, *10*, 22236–22244.

[33] J. Zhao, X. Zou, Y. Zhu, Y. Xu, C. Wang, *Adv. Funct. Mater.* **2016**, *26*, 8103–8110.

[34] L. Fan, R. Ma, Q. Zhang, X. Jia, B. J. A. C. I. E. Lu, *Angew. Chem. Int. Ed.* **2019**, *58*, 10500–10505.

[35] Y. An, H. Fei, G. Zeng, L. Ci, B. Xi, S. Xiong, J. Feng, *J. Power Sources* **2018**, *378*, 66–72.

[36] P. Xiong, X. Zhao, Y. Xu, *ChemSusChem* **2018**, *11*, 202–208.

[37] Y. Xie, H. Zhang, K. Wu, X. Wang, D. Xiong, M. He, *J. Alloys Compd.* **2022**, *910*, 164845.

[38] D. S. Bin, Z. X. Chi, Y. Li, K. Zhang, X. Yang, Y. G. Sun, J. Y. Piao, A. M. Cao, L. J. Wan, *J. Am. Chem. Soc.* **2017**, *139*, 13492–13498.

[39] Y. Wu, J. Cheng, Z. Liang, Y. Tang, T. Qiu, S. Gao, R. Zhong, R. Zou, *Small* **2022**, *18*, 2105767.

[40] B. Cao, Q. Zhang, H. Liu, B. Xu, S. Zhang, T. Zhou, J. Mao, W. K. Pang, Z. Guo, A. Li, *Adv. Energy Mater.* **2018**, *8*, 1801149.

[41] F. Yao, D. T. Pham, Y. H. Lee, *ChemSusChem* **2015**, *8*, 2284–2311.

[42] R. A. Adams, A. Varma, V. G. Pol, *Adv. Energy Mater.* **2019**, *9*, 1900550.

[43] a) see ref. [27]; b) S. Gong, Q. Wang, *J. Phys. Chem. C* **2017**, *121*, 24418–24424; c) Q. Yao, J. Zhang, X. Shi, B. Deng, K. Hou, Y. Zhao, L. Guan, *Electrochim. Acta* **2019**, *307*, 118–128.

[44] E. Olsson, G. Chai, M. Dove, Q. Cai, *Nanoscale* **2019**, *11*, 5274–5284.

[45] X. Xiong, G. Wang, Y. Lin, Y. Wang, X. Ou, F. Zheng, C. Yang, J.-H. Wang, M. Liu, *ACS Nano* **2016**, *10*, 10953–10959.

[46] S. Komaba, W. Murata, T. Ishikawa, N. Yabuuchi, T. Ozeki, T. Nakayama, A. Ogata, K. Gotoh, K. Fujiwara, *Adv. Funct. Mater.* **2011**, *21*, 3859–3867.

[47] Z. Jian, Z. Xing, C. Bommier, Z. Li, X. Ji, *Adv. Energy Mater.* **2016**, *6*, 1501874.

[48] L. Zhong, W. Zhang, S. Sun, L. Zhao, W. Jian, X. He, Z. Xing, Z. Shi, Y. Chen, H. N. Alshareef, X. Qiu, *Adv. Funct. Mater.* **2023**, *33*, 2211872.

[49] C. Chen, Z. Wang, B. Zhang, L. Miao, J. Cai, L. Peng, Y. Huang, J. Jiang, Y. Huang, L. Zhang, J. Xie, *Energy Storage Mater.* **2017**, *8*, 161–168.

[50] C. Hu, L. Dai, *Adv. Mater.* **2017**, *29*, 1604942.

[51] M. Chen, W. Wang, X. Liang, S. Gong, J. Liu, Q. Wang, S. Guo, H. Yang, *Adv. Energy Mater.* **2018**, *8*, 1800171.

[52] S. Chong, L. Yuan, T. Li, C. Shu, S. Qiao, S. Dong, Z. Liu, J. Yang, H. K. Liu, S. X. Dou, W. Huang, *Small* **2022**, *18*, 2104296.

[53] J. Yang, Z. Ju, Y. Jiang, Z. Xing, B. Xi, J. Feng, S. Xiong, *Adv. Mater.* **2018**, *30*, 1700104.

[54] R. C. Cui, B. Xu, H. J. Dong, C. C. Yang, Q. Jiang, *Adv. Sci.* **2020**, *7*, 1902547.

[55] Z. Jian, S. Hwang, Z. Li, A. S. Hernandez, X. Wang, Z. Xing, D. Su, X. Ji, *Adv. Funct. Mater.* **2017**, *27*, 1700324.

[56] X. Wang, K. Han, D. Qin, Q. Li, C. Wang, C. Niu, L. Mai, *Nanoscale* **2017**, *9*, 18216–18222.

[57] S. Trasatti, G. Buzzanca, *J. Electroanal. Chem. Interfacial Electrochem.* **1971**, *29*, A1–A5.

[58] V. Augustyn, P. Simon, B. Dunn, *Energy Environ. Sci.* **2014**, *7*, 1597–1614.

[59] T. C. Liu, W. Pell, B. Conway, S. Roberson, *J. Electrochem. Soc.* **1998**, *145*, 1882–1888.

[60] X. Zhao, P. Xiong, J. Meng, Y. Liang, J. Wang, Y. Xu, *J. Mater. Chem. A* **2017**, *5*, 19237–19244.

[61] Y. Xu, C. Zhang, M. Zhou, Q. Fu, C. Zhao, M. Wu, Y. Lei, *Nat. Commun.* **2018**, *9*, 1720.

[62] see ref. [12]

[63] H. He, D. Huang, Y. Tang, Q. Wang, X. Ji, H. Wang, Z. Guo, *Nano Energy* **2019**, *57*, 728–736.

[64] W. Wang, J. Zhou, Z. Wang, L. Zhao, P. Li, Y. Yang, C. Yang, H. Huang, S. Guo, *Adv. Energy Mater.* **2018**, *8*, 1701648.

[65] C. Ma, X. Tang, J. Jiang, Z. Ma, H. Li, H. Ben, X.-Z. Yuan, *Chem. Eng. J.* **2023**, *454*, 140116.

[66] Y. Qiao, J. Yi, S. Wu, Y. Liu, S. Yang, P. He, H. Zhou, *Joule* **2017**, *1*, 359–370.

[67] see ref. [13]

[68] A. Mahmood, S. Li, Z. Ali, H. Tabassum, B. Zhu, Z. Liang, W. Meng, W. Aftab, W. Guo, H. Zhang, *Adv. Mater.* **2019**, *31*, 1805430.

[69] J. Wang, Y. Qin, L. Li, S. Zhang, X. Pei, Z. Niu, X.-C. Zheng, D. Li, *Chem. Eng. J.* **2023**, *457*, 141253.

[70] K. Gong, F. Du, Z. Xia, M. Durstock, L. Dai, *Science* **2009**, *323*, 760–764.

[71] D. Yu, K. Goh, H. Wang, L. Wei, W. Jiang, Q. Zhang, L. Dai, Y. Chen, *Nat. Nanotechnol.* **2014**, *9*, 555.
[72] A. Khurram, M. He, B. M. Gallant, *Joule* **2018**, *2*, 2649–2666.
[73] Z. Ju, S. Zhang, Z. Xing, Q. Zhuang, Y. Qiang, Y. Qian, *ACS Appl. Mater. Interfaces* **2016**, *8*, 20682–20690.
[74] Z. Tai, Y. Liu, Q. Zhang, T. Zhou, Z. Guo, H. K. Liu, S. X. Dou, *Green Energy & Environ.* **2017**, *2*, 278–284.
[75] A. P. Cohn, N. Muralidharan, R. Carter, K. Share, L. Oakes, C. L. Pint, *J. Mater. Chem. A* **2016**, *4*, 14954–14959.
[76] K. Share, A. P. Cohn, R. Carter, B. Rogers, C. L. Pint, *ACS Nano* **2016**, *10*, 9738–9744.
[77] Z. Ju, P. Li, G. Ma, Z. Xing, Q. Zhuang, Y. Qian, *Energy Storage Mater.* **2018**, *11*, 38–46.
[78] X. Qi, K. Huang, X. Wu, W. Zhao, H. Wang, Q. Zhuang, Z. Ju, *Carbon* **2018**, *131*, 79–85.
[79] R. A. Adams, J. M. Syu, Y. Zhao, C. T. Lo, A. Varma, V. G. Pol, *ACS Appl. Mater. Interfaces* **2017**, *9*, 17872–17881.
[80] Y. Li, R. A. Adams, A. Arora, V. G. Pol, A. M. Levine, R. J. Lee, K. Akato, A. K. Naskar, M. P. Paranthaman, *J. Electrochem. Soc.* **2017**, *164*, A1234–A1238.
[81] see ref. [34]
[82] X. Zhou, L. Chen, W. Zhang, J. Wang, Z. Liu, S. Zeng, R. Xu, Y. Wu, S. Ye, Y. Feng, X. Cheng, Z. Peng, X. Li, Y. Yu, *Nano Lett.* **2019**, *19*, 4965–4973.
[83] W. Cao, E. Zhang, J. Wang, Z. Liu, J. Ge, X. Yu, H. Yang, B. Lu, *Electrochim. Acta* **2019**, *293*, 364–370.
[84] C. Shen, K. Yuan, T. Tian, M. Bai, J.-G. Wang, X. Li, K. Xie, Q.-G. Fu, B. Wei, *ACS Appl. Mater. Interfaces* **2019**, *11*, 5015–5021.
[85] Y. Zhang, L. Yang, Y. Tian, L. Li, J. Li, T. Qiu, G. Zou, H. Hou, X. Ji, *Mater. Chem. Phys.* **2019**, *229*, 303–309.
[86] N. Xiao, X. Zhang, C. Liu, Y. Wang, H. Li, J. Qiu, *Carbon* **2019**, *147*, 574–581.
[87] A. Mahmood, S. Li, Z. Ali, H. Tabassum, B. Zhu, Z. Liang, W. Meng, W. Aftab, W. Guo, H. Zhang, *Adv. Mater.* **2019**, *31*, 1805430.
[88] H. Huang, R. Xu, Y. Feng, S. Zeng, Y. Jiang, H. Wang, W. Luo, Y. Yu, *Adv. Mater.* **2020**, *32*, 1904320.
[89] W. Feng, Y. Cui, W. Liu, H. Wang, Y. Zhang, Y. Du, S. Liu, H. Wang, X. Gao, T. Wang, *ACS Nano* **2020**, *14*, 4938–4949.
[90] L. Tao, Y. Yang, H. Wang, Y. Zheng, H. Hao, W. Song, J. Shi, M. Huang, D. Mitlin, *Energy Storage Mater.* **2020**, *27*, 212–225.
[91] J. Ding, H. Zhang, H. Zhou, J. Feng, X. Zheng, C. Zhong, E. Paek, W. Hu, D. Mitlin, *Adv. Mater.* **2019**, *31*, 1900429.
[92] J. Li, Y. Li, X. Ma, K. Zhang, J. Hu, C. Yang, M. Liu, *Chem. Eng. J.* **2020**, *384*, 123328.
[93] X. Hu, Y. Liu, J. Chen, L. Yi, H. Zhan, Z. Wen, *Adv. Energy Mater.* **2019**, *9*, 1901533.
[94] J. Ruan, F. Mo, Z. Chen, M. Liu, S. Zheng, R. Wu, F. Fang, Y. Song, D. Sun, *Adv. Energy Mater.* **2020**, *10*, 1904045.
[95] Y. Yi, J. Li, W. Zhao, Z. Zeng, C. Lu, H. Ren, J. Sun, J. Zhang, Z. Liu, *Adv. Funct. Mater.* **2020**, *30*, 2003039.
[96] X. Sui, X. Huang, H. Pu, Y. Wang, J. Chen, *Nano Energy* **2021**, *83*, 105797.
[97] Q. Jiang, L. Wang, W. Zhao, X. Xu, Z. Li, Y. Li, T. Zhou, J. Hu, *Chem. Eng. J.* **2022**, *433*, 133539.
[98] J. Zhu, Y. Li, B. Yang, L. Liu, J. Li, X. Yan, D. He, *Small* **2018**, *14*, 1801836.
[99] J. A. Read, A. V. Cresce, M. H. Ervin, K. Xu, *Energy Environ. Sci.* **2014**, *7*, 617–620.
[100] a) H. Kim, J. Hong, Y. U. Park, J. Kim, I. Hwang, K. Kang, *Adv. Funct. Mater.* **2015**, *25*, 534–541; b) B. Jache, P. Adelhelm, *Angew. Chem.* **2014**, *126*, 10333–10337.
[101] M. Beidaghi, Y. Gogotsi, *Energy Environ. Sci.* **2014**, *7*, 867–884.
[102] K. Kubota, M. Dahbi, T. Hosaka, S. Kumakura, S. Komaba, *Chem. Rec.* **2018**, *18*, 459–479.
[103] K. Beltrop, S. Beuker, A. Heckmann, M. Winter, T. Placke, *Energy Environ. Sci.* **2017**, *10*, 2090–2094.
[104] L. Fan, Q. Liu, S. Chen, K. Lin, Z. Xu, B. Lu, *Small* **2017**, *13*, 1701011.
[105] B. Ji, F. Zhang, N. Wu, Y. Tang, *Adv. Energy Mater.* **2017**, *7*, 1700920.
[106] see ref. [104]
[107] L. Fan, K. Lin, J. Wang, R. Ma, B. Lu, *Adv. Mater.* **2018**, *30*, 1800804.
[108] a) J. Chen, B. Yang, H. Li, P.-J. Ma, X. Yan, *J. Mater. Chem. A* **2019**, *7*, 9247–9252; b) Y. Luan, R. Hu, Y. Fang, K. Zhu, K. Cheng, J. Yan, K. Ye, G. Wang, D. Cao, *Nano-Micro Lett.* **2019**, *11*, 30.
[109] B. Dunn, H. Kamath, J.-M. Tarascon, *Science* **2011**, *334*, 928–935.
[110] D. Lin, Y. Liu, Y. Cui, *Nat. Nanotechnol.* **2017**, *12*, 194.
[111] N. Xiao, R. T. Rooney, A. A. Gewirth, Y. Wu, *Angew. Chem.* **2018**, *130*, 1241–1245.
[112] L. Zhang, Y. Tang, Q. Liu, T. Yang, C. Du, P. Jia, Z. Wang, Y. Tang, Y. Li, T. Shen, *Nano Energy* **2018**, *53*, 544–549.
[113] W. Yu, K. C. Lau, Y. Lei, R. Liu, L. Qin, W. Yang, B. Li, L. A. Curtiss, D. Zhai, F. Kang, *ACS Appl. Mater. Interfaces* **2017**, *9*, 31871–31878.
[114] K. Lu, H. Zhang, F. Ye, W. Luo, H. Ma, Y. Huang, *Energy Storage Mater.* **2019**, *16*, 1–5.
[115] R. Paul, F. Du, L. Dai, Y. Ding, Z. L. Wang, F. Wei, A. Roy, *Adv. Mater.* **2019**, *31*, 1805598.
[116] Y. Yao, R. Xu, M. Chen, X. Cheng, S. Zeng, D. Li, X. Zhou, X. Wu, Y. Yu, *ACS Nano* **2019**, *13*, 4695–4704.
[117] N. Xiao, X. Ren, W. D. McCulloch, G. Gourdin, Y. Wu, *Acc. Chem. Res.* **2018**, *51*, 2335–2343.
[118] W. Wang, Y. Wang, C.-H. Wang, Y.-W. Yang, Y.-C. Lu, *Energy Storage Mater.* **2021**, *36*, 341–346.
[119] a) X. Ren, K. C. Lau, M. Yu, X. Bi, E. Kreidler, L. A. Curtiss, Y. Wu, *ACS Appl. Mater. Interfaces* **2014**, *6*, 19299–19307; b) N. Xiao, X. Ren, M. He, W. D. McCulloch, Y. Wu, *ACS Appl. Mater. Interfaces* **2017**, *9*, 4301–4308; c) X. Ren, M. He, N. Xiao, W. D. McCulloch, Y. Wu, *Adv. Energy Mater.* **2017**, *7*, 1; d) S. Sankarasubramanian, V. K. Ramani, *J. Phys. Chem. C* **2018**, *122*, 19319–19327.
[120] L. Qie, Y. Lin, J. W. Connell, J. Xu, L. Dai, *Angew. Chem. Int. Ed.* **2017**, *56*, 6970–6974.
[121] W. Zhang, C. Hu, Z. Guo, L. Dai, *Angew. Chem. Int. Ed.* **2020**, *59*, 3470–3474.
[122] X. Li, G. Qi, J. Zhang, J. Cheng, B. Wang, *Adv. Funct. Mater.* **2022**, *32*, 2105029.
[123] P. Xiong, X. Han, X. Zhao, P. Bai, Y. Liu, J. Sun, Y. Xu, *ACS Nano* **2019**, *13*, 2536–2543.
[124] R. Xu, Y. Yao, H. Wang, Y. Yuan, J. Wang, H. Yang, Y. Jiang, P. Shi, X. Wu, Z. Peng, Z. S. Wu, J. Lu, Y. Yu, *Adv. Mater.* **2020**, *32*, 2003879.
[125] H. Wang, W. Zhang, H. Liu, Z. Guo, *Angew. Chem. Int. Ed.* **2016**, *55*, 3992–3996.
[126] Y. Ding, J. Cai, Y. Sun, Z. Shi, Y. Yi, B. Liu, J. Sun, *ACS Nano* **2022**, *16*, 3373–3382.
[127] W. D. McCulloch, X. Ren, M. Yu, Z. Huang, Y. Wu, *ACS Appl. Mater. Interfaces* **2015**, *7*, 26158–26166.
[128] a) J. Zhang, Y. Li, L. Zhu, X. Wang, J. Tu, *Energy Storage Mater.* **2021**, *41*, 606–613; b) Y. Zhong, S. Zhou, Q. He, A. Pan, *Energy Storage Mater.* **2022**, *45*, 48–73.
[129] a) J. Park, J. Lee, M. H. Alfaruqi, W.-J. Kwak, J. Kim, J.-Y. Hwang, *J. Mater. Chem. A* **2020**, *8*, 16718–16737; b) J. Park, Y. Jeong, M. H. Alfaruqi, Y. Liu, X. Xu, S. Xiong, M.-G. Jung, H.-G. Jung, J. Kim, J.-Y. Hwang, Y.-K. Sun, *ACS Energy Lett.* **2022**, *7*, 401–409.

[130] a) P. Liu, H. Hao, H. Celio, J. Cui, M. Ren, Y. Wang, H. Dong, A. R. Chowdhury, T. Hutter, F. A. Perras, J. Nanda, J. Watt, D. Mitlin, *Adv. Mater.* **2022**, *34*, 2105855; b) P. Li, T. Xu, P. Ding, J. Deng, C. Zha, Y. Wu, Y. Wang, Y. Li, *Energy Storage Mater.* **2018**, *15*, 8–13.
[131] L. Qin, Y. Lei, H. Wang, J. Dong, Y. Wu, D. Zhai, F. Kang, Y. Tao, Q. H. Yang, *Adv. Energy Mater.* **2019**, *9*, 1901427.
[132] Z. Wei, A. Wang, X. Guan, G. Li, Z. Yang, C. Huang, J. Zhang, L. Ren, J. Luo, X. Liu, *Energy Environ. Mater.* **2022**, *5*, 1278–1284.
[133] J. Meng, H. Zhu, Z. Xiao, X. Zhang, C. Niu, Y. Liu, G. Jiang, X. Wang, F. Qiao, X. Hong, F. Liu, Q. Pang, L. Mai, *ACS Nano* **2022**, *16*, 7291–7300.
[134] X. Guo, Y. Ding, H. Gao, J. B. Goodenough, G. Yu, *Adv. Mater.* **2020**, *32*, 2000316.
[135] L. Zhang, X. Xia, Y. Zhong, D. Xie, S. Liu, X. Wang, J. Tu, *Adv. Mater.* **2018**, *30*, 1804011.
[136] W. Yuan, T. Ding, P. Mou, Y. Luo, L. Li, Y. Chen, X. Chen, J. Shu, L. Zhang, *Adv. Funct. Mater.* **2023**, *33*, 2209774.
[137] a) J. Wang, W. Yan, J. Zhang, *Nano Energy* **2022**, *96*, 107131; b) F. Qiao, J. Meng, J. Wang, P. Wu, D. Xu, Q. An, X. Wang, L. Mai, *J. Mater. Chem. A* **2021**, *9*, 23046–23054.
[138] Y. Xie, J. Hu, Z. Han, H. Fan, J. Xu, Y. Lai, Z. Zhang, *Nano Res.* **2020**, *13*, 3137–3141.
[139] P. Liu, Y. Wang, Q. Gu, J. Nanda, J. Watt, D. Mitlin, *Adv. Mater.* **2020**, *32*, 1906735.
[140] Y. Zhang, A. Bahi, F. Ko, J. Liu, *Small* **2022**, *18*, 2107186.
[141] see ref. [110]
[142] D. Lin, Y. Liu, Z. Liang, H.-W. Lee, J. Sun, H. Wang, K. Yan, J. Xie, Y. Cui, *Nat. Nanotechnol.* **2016**, *11*, 626.
[143] R. P. Joshi, B. Ozdemir, V. Barone, J. E. Peralta, *J. Phys. Chem. Lett.* **2015**, *6*, 2728–2732.
[144] W. Zuo, R. Li, C. Zhou, Y. Li, J. Xia, J. Liu, *Adv. Sci.* **2017**, *4*, 1600539.
[145] H. Wang, D. Zhai, F. Kang, *Energy Environ. Sci.* **2020**, *13*, 4583–4608.
[146] P. Peljo, H. H. Girault, *Energy Environ. Sci.* **2018**, *11*, 2306–2309.

Manuscript received: June 26, 2023
Accepted manuscript online: July 16, 2023
Version of record online: August 3, 2023